https://doi.org/10.15407/ufm.24.02.282

V.B. TARELNYK [1,*], O.P. GAPONOVA [2,], N.V. TARELNYK [1], and O.M. MYSLYVCHENKO [3]**

[1] Sumy National Agrarian University,
160 Gerasym Kondratiev Str., UA-40021 Sumy, Ukraine
[2] Sumy State University,
2 Rymsky-Korsakov Str., UA-40007 Sumy, Ukraine
[3] I.M. Frantsevych Institute for Problems of Materials Science
of the N.A.S. of Ukraine,
3, Omeljan Pritsak Str., UA-03142 Kyiv, Ukraine

* tarelnik@i.ua, ** gaponova@pmtkm.sumdu.edu.ua

ALUMINIZING OF METAL SURFACES BY ELECTRIC-SPARK ALLOYING

The analysis of the influence of the parameters of electrospark alloying with an aluminium electrode on the quality (roughness, microstructure of the coating, its continuity, phase composition, and microhardness) of the aluminized layer is presented. The effect of finishing methods after aluminizing is evaluated. The heat resistance of the obtained coatings is studied. Metallographic analysis shows that the coating consists of three sections: a 'white' layer, a diffusion zone, and the base metal. With an increase in the discharge energy, such quality parameters of the surface layer as thickness, microhardness of both a 'white' layer and a transition zone, and roughness are increased. The continuity of a 'white' layer at the discharge energy $W_p = 0.52$ J is low (of 50–60%); with a subsequent increase in the discharge energy, it increases and, at $W_p = 6.8$ J, it is of 100%. An increase in the discharge energy during electric-spark alloying (ESA) leads to a change in the chemical and phase compositions of the layer: at low discharge energies, a layer is formed, consisting mainly of α-Fe and aluminium oxides. As W_p increases, the layer consists of iron and aluminium intermetallic compounds, as well as free aluminium, that is confirmed by the data of local x-ray microanalysis. For practical application, it is possible to recommend the process of aluminizing by the ESA method, using the modes (discharge energy in the range of 4.6–6.8 J and productivity of 2.0–3.0 cm^2/min). Such

Citation: V.B. Tarelnyk, O.P. Gaponova, N.V. Tarelnyk, and O.M. Myslyvchenko, Aluminizing of Metal Surfaces by Electric-Spark Alloying, *Progress in Physics of Metals*, **24**, No. 2: 282–318 (2023)

process provides the formation of a 'white' layer with a thickness of 70–130 μm, microhardness of 5000–7500 MPa, roughness (R_a) of 6–9 μm, and continuity of 95–100%. In order to increase the thickness of the aluminized layer, it is recommended to preliminarily apply grease containing aluminium powder to the steel surface and, without waiting for it to dry, carry out ESA with an aluminium electrode. In this case, the coating continuity is of 100%, the layer thickness is of up to 200 μm, and the microhardness is of 4500 MPa. The paper presents the results of study of the quality parameters of multicomponent aluminium-containing coatings of Al–S, Al–C–S, and Al–C–B systems. Replacing the aluminium electrode with graphite one leads to a decrease in the thickness and continuity of a 'white' layer, respectively, to 50 μm and 30%. In turn, the microhardness on the surface increases to 9000 MPa. The addition of 0.7 boron to the consistency substance leads to an increase in the thickness and continuity of a 'white' layer, respectively, up to 60 μm and 70%. The microhardness on the surface rises to 12000 MPa. In order to reduce the roughness of the surface layer and to obtain continuous coatings, it is recommended to carry out ESA with an aluminium electrode, but at lower modes.

Keywords: electrospark alloying, coating, aluminizing, microhardness, continuity, roughness, structure, x-ray diffraction analysis, x-ray spectral analysis.

1. Introduction

Thanks to the development of scientific and technological progress (STP), various industries are constantly being improved. Those are metallurgical, oil refining, chemical, aerospace, coal mining, and others. In Ukraine, up to 40% of the industrial potential is occupied by the mechanical engineering, which produces various machines and equipment. With advent of new machines and equipment, there have been being increased the requirements for their parts, which operate under extreme environmental conditions and at constantly increasing operating parameters (pressure, temperature, speed, radiation exposure, *etc.*) Up to a certain time, the problems connected with protecting the parts from various types of wear had been resolved through choosing materials for their manufacture. As a rule, those are expensive and difficult to process steels and alloys.

For example, the sealing rings of face impulse seals (FIS) are entirely made of wear-resistant materials such as tungsten carbide and silicon carbide. The cost of the rings made of these materials reaches hundreds and thousands of US dollars, which determines the high cost of the sealing units in general [1–3].

Taking into consideration that the destruction of a part usually begins from the surface, in recent decades, much attention has been paid to improving the known technologies and developing the new technologies, which can properly change the quality parameters of the part surface layers. For example, a promising way to increase the wear resistance of FIS rings can be the formation of quasi-multilayer coatings,

which combine the lubrication and anti-wear properties, on the working face surfaces. Such coatings can be the combined electrospark coatings that conjoin hard wear-resistant and soft antifriction materials [4, 5].

A new composite material combines the protective properties of the coating with the mechanical strength of the base. A part made of a cheaper and easily workable base material and that possessing a surface layer formed due to the use of progressive, low-energy-intensive and environmentally friendly technology is not inferior in any way, and often, in terms of individual features (durability, cost, consumption of metal-cutting tools and accessories, the presence of alloying elements, *etc.*) is superior to a part made of an integral material. Thus, technological solutions aimed at creating fundamentally new materials with increased surface wear resistance, relatively high strength and viscosity are an urgent problem [6–8].

Currently, designers and technologists abound with a large number of technologies designed to provide a surface layer of a part with the necessary physical, chemical, tribological, and operational properties. So the surfaces of parts are subjected to various types of strengthening to protect them from various types of wear and the negative effects of the environment. Those are as follows: various methods for spraying of metal-ceramic coatings [9–11], depositing coatings of composite materials [12, 13], performing centrifugal reinforcement of steel surface layers with tungsten carbide particles [14], applying the coatings with layers of aluminium oxide [15–17], performing the process of electrochemical chromium plating in flowing electrolyte [18]. To study the damaged coverings, the authors of paper [19] improved the method of processing images of metal structures. A special place among the technologies used to improve the quality features of part surfaces is occupied by chemical-thermal treatment technology (CTT) [20–22].

The CTT combines carburizing, nitriding, nitrocarburizing and a number of other methods.

One of the popular methods of the CTT is an aluminizing process. It is known [23] that in order to provide iron-carbon alloys with increased scale resistance, resistance to atmospheric corrosion, and a number of other properties, the aluminizing method is used. In addition, the complex aluminized coatings [24] are characterized by a high melting point, low density, high modulus of elasticity, heat resistance, resistance to oxidation and ignition. Moreover, recently there has been being emerged a tendency for the use of complex aluminized coatings to create protective and wear-resistant coatings.

There are well-known processes for aluminizing by methods of chemical and thermal treatment [25–27]. According to the classic technology, aluminizing process consists in saturating the surface of a steel part in molten aluminium. At the same time, there are other known

methods for aluminizing process. For example, in work [28], the aluminizing method includes the procedures of applying an aluminium layer on a steel surface (usually by spraying), coating and annealing. In this event, a special attention is paid to the roughness of the surface subject to the aluminizing procedure. Moreover, the availability of oxide films, oil and dust is unacceptable therein. Despite the positive results, the above technology, as well as the classic technology of aluminizing in melts, has a number of disadvantages intrinsic to the CTT technologies.

In addition to the above, the most effective methods for controlling the quality parameters of surface layers include the technologies using the concentrated energy flows (CEF) for processing the material, for example, plasma technologies (spraying [29–31] and plasma processing [32, 33]), and laser processing [34–36]. In the course of the CEF processing, there occur non-equilibrium heating and cooling conditions, which lead to the formation of a surface layer structure, which is fundamentally different from that provided by the traditional processing methods. The electrospark alloying (ESA) method is one of the most promising modern technologies, which are capable of controlling the parameters of a part surface quality.

Carried out by using the CEF, the ESA method provides the formation of the nanolevel surface-layer structures having unique physical, mechanical, and tribological properties [37].

When the electrodes are approaching each other, the surfaces are being subjected to the local actions of the shock wave high pressures and temperatures [38, 39].

At the same time, there occurs the anode instantaneous heating rate of, and a drop or solid particle of the anode material starts moving to the cathode. While flying from the anode to the cathode, the fragments have been being heated to a high temperature. The temperature of the short-term heating of the surface micro-volumes reaches $(5–7)\cdot 10^3$ K. The spark discharge occurs in microscopically small volumes and lasts of 50–400 microseconds. On the cathode, there have been being formed the impressions and micro-baths, wherein the particles of the anode and cathode have been interacting with each other and the environment, activating the diffusion processes. This results in the formation of the new phases and a change in the structure of the surface layer.

As compared to the traditional methods of the surface treatment, among the main advantages of the ESA technology, it is reasonable to note its environmental and technogenic safety, the possibility of its application in local areas, which requires no protection of adjacent surfaces from the negative impact of the ESA process, a high degree of the applied metal adhesion, the absence of contractions and deformation, ability to be built into any technological process, *etc.* [40, 41].

Practically, in all known literature and patent sources, the disadvantages of the ESA process include as follows: increased surface roughness, in some cases, porosity up to 2 μm, small coating thickness, reduced fatigue strength, *etc.* [42, 43]. At the same time, it should be noted that in some cases, the specified disadvantages appear as advantages.

For certain technologies of strengthening and restoring the parts (various spraying methods, application of metal–polymer materials (MPM), *etc.*), for better adhesion of the applied materials to the substrate, it is necessary to create some roughness thereon, using any known methods and means (grinding wheels, lathe cutters, *etc.*) [44]. Formed by the above methods, the roughness protrusions and depressions are of sharp shape. This event leads to the appearance of the stress concentrators on the surface of the part, which becomes the reason for the decrease in the part fatigue strength.

Having been processed by the ESA method, the surface roughness has another sloping profile without sharp differences [45]. In recent years, this made it possible to use the ESA method in the combined ESA technologies with the procedure of applying metal–polymer materials (MPM) [46].

The analysis of the operation of the parts working under difficult operating conditions showed that the vast majority of them do not require 'thick' layers as strengthened surface layers. The wear of the order of 0.02 mm of the surface of the neck of the shaft for a rotary machine (compressor, pump, centrifuge, electric motor, *etc.*) or of the surface in contact with that of the part pressed onto the shaft results in the destruction of the press joint. In turn, at 'finishing' ESA, it is possible to obtain the wear-resistant coatings of high quality (100% continuity and the thickness of up to 1.0 mm and even more), for example, at restoring the surfaces of screw compressor belts [47].

As for the presence of pores in the coatings, this is also an advantage of the ESA method. For many years, the technologists have been looking for the ways to create such a structure of the surface layer, in the pores of which a lubricant could be kept in the friction pairs [48, 49], for example, in the bearing necks of the shafts [50, 51].

The paper of [52] represents the results of an investigation of the corrosion resistance of the aluminium coatings on the St3 steel obtained in molten aluminium. It is shown that with an increase in the thickness of the coating obtained by the ESA method with an aluminium electrode, the resistance to atmospheric corrosion increases. The authors also note that the porosity of the electrospark aluminium coatings is not a limiting factor. Electrochemical corrosion develops in the pore spaces in the presence of electrolyte (moisture). At the same time, the coating serves as the anode, and the steel as the cathode. Under the condition of a porous coating, the base metal has been being protected electrochemi-

cally until the layer dissolves. The cathode has been being protected with the use of an anode mechanism. In the case of the non-porous electrospark aluminium coatings, in addition to the above-described mechanism, there is also a shielding mechanism for the protection against corrosion destruction. This protection increases with increasing oxide layers on the aluminium coatings.

As shown in works [53, 54], the electrospark aluminium coatings reliably protect steel in phosphoric acid and water-salt environments.

Authors of Ref. [55] proposed a method for applying the coatings that includes the procedure of electrospark alloying a metal surface with the use of an aluminium electrode. The structure and composition of the coatings were studied using the methods of electron microscopy, x-ray structural and micro-x-ray spectral analyses. The researched technology has some advantages as compared to the other already known technologies. However, such an ESA technology with the use of an aluminium electrode is performed in a protective environment (argon), which significantly increases the costs of the process, and in addition, the specified technology is used only for titanium parts.

Therefore, the development of a new aluminizing technology based on the ESA method, the study of the influence of the process energy parameters on the structural and phase state of the surface layer, as well as the properties provided by the aluminized layer, are topical. The analysis of the relevant literature and patent sources, as well as a number of the studies, which had been conducted by the authors of this paper, showed the promising nature of the investigations aimed at improving the aluminizing technology at the cost of its implementation by the electrospark alloying technologies.

Thus, the available data on phase and structural transformations in the surface layers of steels and various metals during the ESA process with the use of an aluminium electrode-tool, the data on the correlation dependences between the parameters of the ESA process and the structural changes in the metal surfaces give rise to the need in the analysis of the accumulated experience, the systematization of the literary and patent sources in of this area, and setting targets for subsequent studies.

The objectives of this work are the following:

(i) to investigate the influence of the parameters of electrospark alloying (discharge energy and alloying productivity) with an aluminium electrode on the quality (roughness and microstructure of the coating, its continuity, phase composition and microhardness) of the alloyed layer;

(ii) to analyse the influence of the methods of the finishing surface treatment of parts after aluminizing on the quality of the coating;

(iii) to conduct the comparative heat resistance tests of the aluminized coatings obtained by the classical technology (in molten aluminium) and ESA with the use of an aluminium electrode;

(iv) to investigate the quality parameters of the multi-component composite coatings.

2. Methodology

To determine the influence of the energy parameters of the ESA equipment on the qualitative parameters of the coatings, the samples were made of steel 20 and steel 40 with the size of 15×15×8 mm, which were coated with the use of an aluminium electrode at the Elytron 52A model using different modes. Moreover, each ESA mode corresponded to its own discharge energy and productivity that is, the area of the formed coating per unit of time (Table 1).

After the ESA process with the use of the aluminium electrode, to reduce the surface roughness, the alloying process was carried out with the use of the same electrode or graphite, but at lower modes.

The surface roughness after the ESA process was measured by taking and processing the profilograms at the profilograph-profilometer of 201 model of the Caliber plant production.

The metallographic analysis of the coatings was performed using the MIM-7 optical microscope and the JEOL JSM 7100f electron microscope; the durometric research was fulfilled at the PMT-3 device.

X-ray radiographic examination was carried out under the atmosphere of CuK_α radiation at the PROTO AXRD diffractometer equipped with a silicon point detector (SPD). The diffraction patterns were taken using the step-by-step scanning method. The scanning step was 0.050; the exposure time at the point was 2 s. The experimental results were processed using the program for the full-profile analysis of the x-ray spectra from the mixture of polycrystalline phase components Powdercell 2.4. Due to the multiphase nature and the superposition of a num-

Table 1. **Dependence of the ESA productivity on the discharge energy [59]**

Discharge energy (W_p), J	0.52	1.3	2.6	4.6	6.8
Productivity, cm^2/min	1.0–1.3	1.3–1.5	1.5–2.0	2.0–2.5	2.5–3.0

Table 2. **The characteristic features of the process for aluminizing the samples of steel 20 [73]**

No. series	Viscous substance composition	Alloying electrode (anode)
1	33.3% S + 56% Al (mass.%)	aluminium
2	33.3% S + 56% Al (mass.%)	graphite
3	33.3% S + 56% Al + 0.7% B (mass.%)	graphite

ber of peaks, their separation was carried out by approximating the diffraction maxima with the Pseudo-Voigt 2 function. Using the least squares method, the best composability was achieved between the experimental and approximating profiles, taking into account the doublet of CuK_α radiation.

To study the distribution of the elements over the depth of the layer, based on the detection of the characteristic x-ray radiation excited by the electron beam of the chemical elements being present in the microvolume, a local x-ray microanalysis was carried out. For this, an electron microscope equipped with an x-ray spectral microanalyser, ISIS 300 Oxford instruments, was used.

In order to increase the thickness of the high-quality structural steel 20 layer aluminized by the ESA method, a viscous substance in the form of a sulphuric ointment with 33.3% sulphur content was applied onto the surfaces of the $15\times15\times8$ mm sized samples. Before the application, the aluminium powder of the PAD-0 mark (GOST 5494-95 was added to the sulfuric ointment. The above aluminium powder is used in powder metallurgy for coating applications by melting down on steel surfaces. The maximum amount of the aluminium powder wanted to add to the colloidal substance was 56%, a further increase led to a decrease in adhesion.

After that, without waiting for drying the viscous substance on the surface of the samples, the ESA process was performed with an aluminium electrode using the Elitron-52A model unit. The rods of $\varnothing$4 mm and length of 45 mm made of the SvA99 (GOST 7871-75) grade aluminium wire were used as the tool electrodes.

To study the effect of carbon on the properties of the coating being formed, the alloying process of the viscous substance of the composition described above was carried out with the use of an electrode made of the graphite of EG-4 grade.

To increase the microhardness of the surface layer of the sample, boron powder was added to the viscous substance in the amount of 0.7%.

The discharge energy (W_p) during the ESA of all series of the samples was 6.8 J. Thus, the three series of the samples made of steel 20 were studied. The characteristics of those are summarized in Table 2.

The investigation of the formed surface layer structures, surface roughness and microhardness measurements were carried out at the equipment and according to the methods described above.

3. Results and Discussions

3.1. Evaluating Quality Parameters of the Surface Layer after Aluminizing via ESA

The microstructures of the aluminium coatings on steel 20 depending on the discharge energy (W_p) are shown in Fig. 1.

The metallographic analysis of the obtained coatings showed that the microstructure consists of three (3) zones: (1) the 'white' layer is a layer, which cannot be etched by ordinary etchants; (2) the transition zone or the diffusion zone; (3) the base metal having a ferrite–pearlite structure.

Table 3 shows the sizes of the microstructure zones depending on the discharge energy. At the low ESA modes (W_p = 0.52 J), a thin layer of the transition zone with a thickness of 20–30 microns is formed. Its continuity tends to 100%. There are separate areas of the 'white' layer (up to 60%) with a thickness of 10–12 microns. As the discharge energy increases, the thicknesses of the 'white' layer and the transition zone increase. At W_p = 1.30 and 4.60 J, the thicknesses of the 'white' layer and the transition zone are respectively equal to 30–50 μm, 30–40 μm and 50–70 μm, 40–60 μm (Table 3). With strengthening the ESA mode, the continuity of the surface layer increases. Thus, at W_p = 2.6 J, the continuity of the diffusion layer tends to 100%, and, that of the 'white' layer, the continuity tends to 85%.

Figure 2 presents the results of the durometric analysis of the microhardness distribution for the aluminized coatings. The maximum hardness has been achieved on the surface and then it has been gradu-

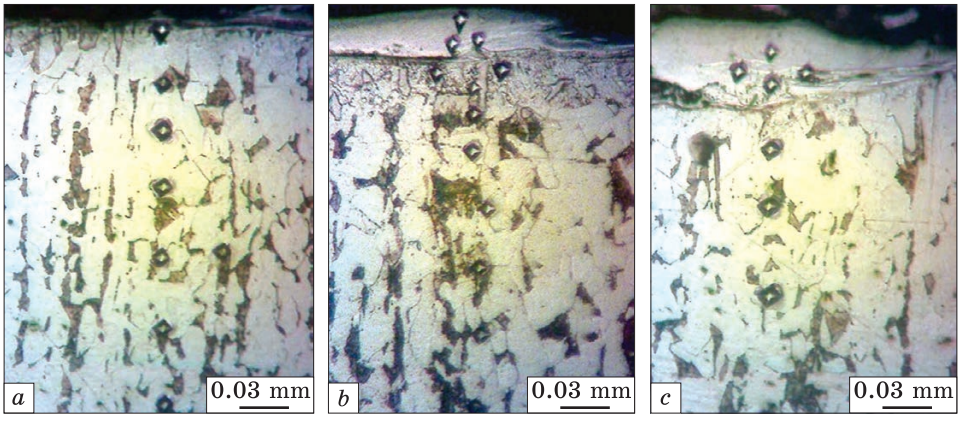

Fig. 1. Cross-sectional microstructures of samples made of steel 20 with aluminium coating obtained by the ESA method: W_p = 0.52 J (*a*), W_p = 1.30 J (*b*), W_p = 2.6 J (*c*) [58]

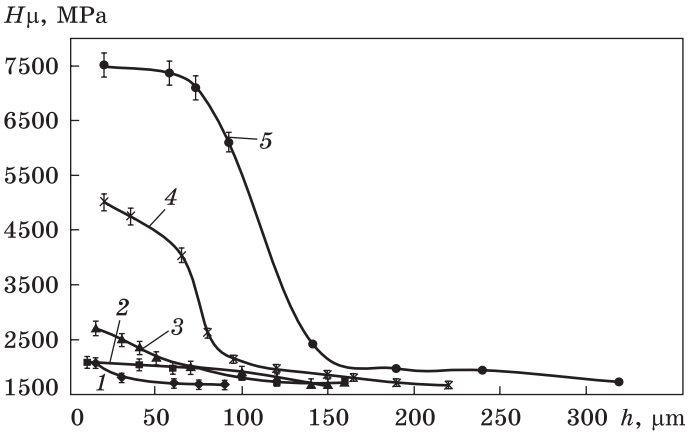

Fig. 2. Dependence of microhardness on the depth of the layer for different processing modes of steel 20: (*1*) W_p = 0.52 J (*1*), W_p = = 1.30 J (*2*), W_p = = 2.6 J (*3*), W_p = = 4.6 J (*4*), W_p = 6.8 J (*5*) [57]

ally decreasing to the microhardness of the base of 1600–1700 MPa. The microhardness values of the coating zones are determined by the energy parameters of the ESA process: the higher the discharge energy, the higher the hardness of the 'white' layer and, accordingly, of the transition zone. Such differences in the microhardness values are due to the diffusion of aluminium into the substrate, as well as a change in the structural and phase composition of the layer.

The analysis of the iron–aluminium state diagram shows [60] that the formation of intermetallics is likely in the ESA layer, which fact is confirmed by the high hardness of the coating. Moreover, the formation

Table 3. **Qualitative parameters of aluminized electrospark coatings on steel [57, 58]**

Discharge energy, J	Thickness, μm		Microhardness, MPa		Roughness, μm			Continuity of the white layer, %
	'white' layer	transition zone	'white' layer	transition zone	R_a	R_z	R_{max}	
Steel 20								
0.52	10–12	20–30	2000 ± 70	1900 ± 50	1.3	2.3	9.3	60
1.30	30–50	30–40	2050 ± 70	1850 ± 80	1.9	6.2	21.6	80
2.60	40–50	30–50	2700 ± 70	2000 ± 200	3.3	9.3	23.2	85
4.60	50–70	40–60	5010 ± 90	2250 ± 200	6.2	16.3	40.6	95
6.8	up to 70	110–130	7270 ± 50	2370 ± 70	9.0	18.1	58.3	100
Steel 40								
0.52	10–15	10–20	2350 ± 50	2000 ± 50	1.6	3.0	8.1	50
2.60	30–70	30–70	3500 ± 50	4500 ± 50	1.9	4.1	11.6	70
6.8	60–130	130–150	7400 ± 70	2390 ± 70	8.1	17.3	49.0	100

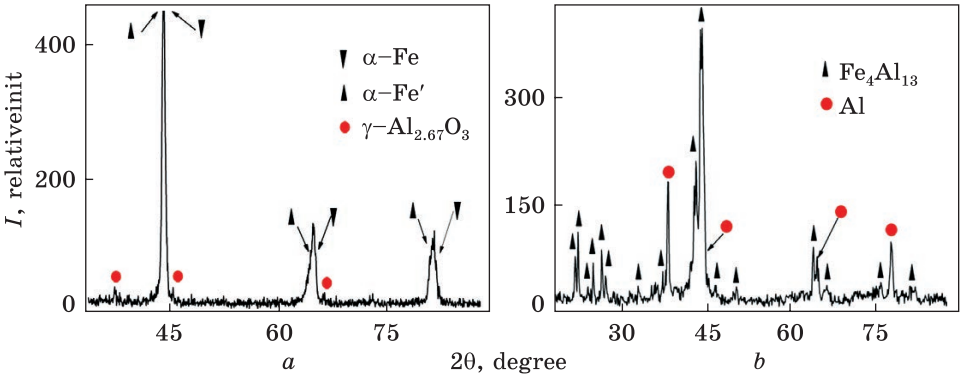

Fig. 3. Diffractograms recorded from the surface of steel 20 after ESA with aluminium at different processing modes: W_p = 0.52 J (*a*), W_p = 1.30 J (*b*) [59]

of nitrides and oxides cannot be excluded [61], because the electric-spark alloying process was carried out in the air. Small volumes of pure electrode material are very likely.

X-ray structure analysis was performed to determine the phase composition of the ESA coatings. The diffractograms recorded from the surface of the sample after aluminizing at W_p = 0.52 J, that is, at the soft mode, indicate to the presence of diffraction maxima of two solid solutions based on a phase with a b.c.c. structure — α-Fe and α′-Fe (229 space group) and aluminium oxide γ-$Al_{2.67}O_4$ (227 space group) (Fig. 3). α-Fe and α′-Fe differ only in the lattice periods that is apparently a consequence of macrostresses arising because of accelerated cooling after the electrospark treatment process (Table 4).

As the discharge energy increases, new phase components appear. If at W_p = 0.52 J, only a solid solution of aluminium in iron and a small amount of aluminium oxide was formed, because the ESA process was carried out in the air, then at W_p = 1.30 J, the conditions were created for the formation of the phase with a monoclinic structure, namely,

Table 4. **Parameters of crystal lattices of phases and quantitative phase analysis after aluminizing process [59]**

ESA mode	Phase	Parameters of phase crystal lattices, Å	Phase content, % by mass
W_p = 0.52 J	α-Fe	a = 2.887	36
	α′-Fe	a = 2.907	47
	γ-$Al_{2.67}O_4$	a = 7.980	17
W_p = 1.30 J	Al	a = 4.056	19
	Fe_4Al_{13}	a = 15.403; b = 8.134; c = 12.473; β = 107.933	81

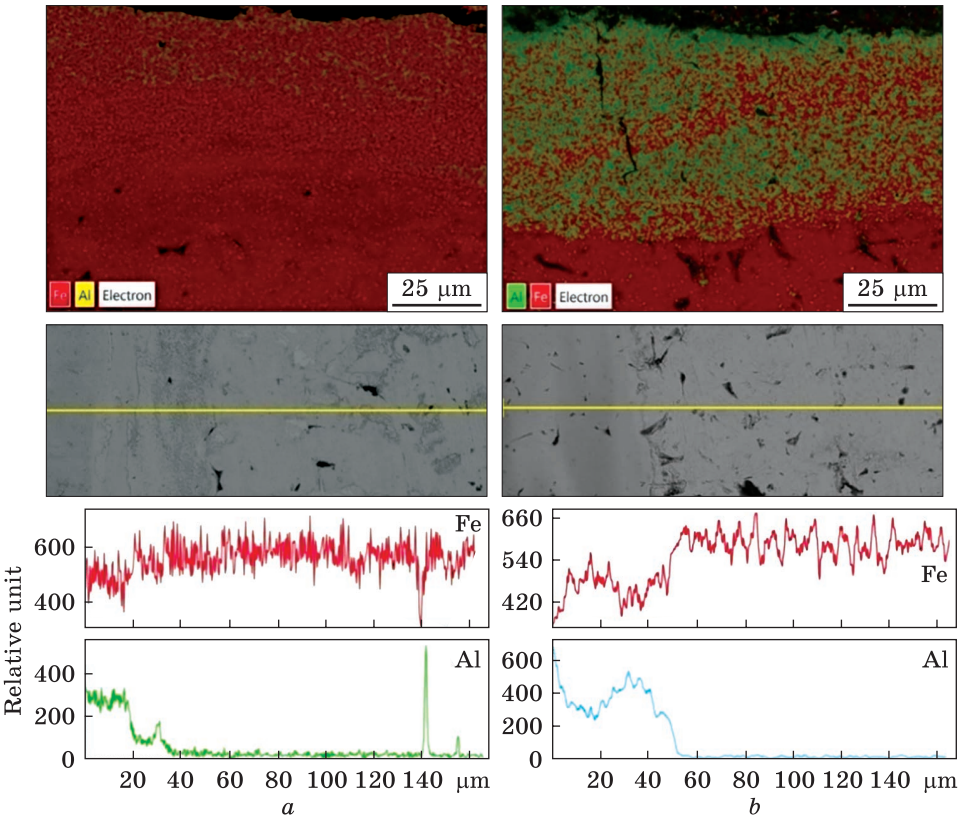

Fig. 4. Concentration curves of the Fe and Al distributions in the coating after the ESA process: W_p = 0.52 J (*a*), W_p = 1.30 J (*b*) [57]

Fe_4Al_{13} (space group 12) and pure aluminium (space group 225). Obviously, the appearance of the intermetallic phases contributes to an increase in the hardness of the coating with an increase in the discharge energy (Fig. 2).

The authors of works [62, 63] and the authors of the present paper have shown by example of Mo–Fe, Cu–Fe pairs that an increase in the discharge energy contributes to the growth of the coating thickness and the enlargement of the diffusion zone between the coating and the substrate.

At the values of W_p = 0.52 J and W_p = 1.30 J, the dimensions of the diffusion zone of aluminium in iron are of 34 and 50 μm, respectively, and the content of aluminium in iron increases (Fig. 4). Thus, at W_p = = 1.30 J, a thin layer of up to 4 microns is formed on the surface, and the aluminium content thereof is approximately of 1.5–2 times higher. The presence of free aluminium in the layer is confirmed by the x-ray structural analysis data (Table 4).

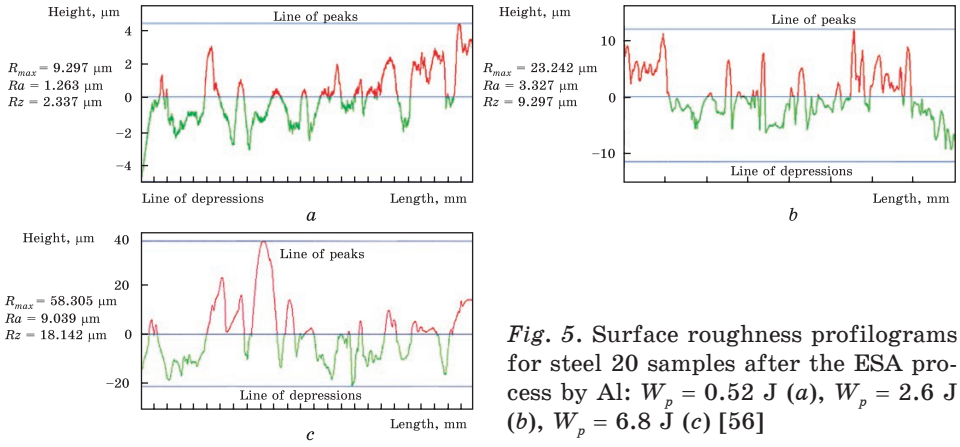

Fig. 5. Surface roughness profilograms for steel 20 samples after the ESA process by Al: W_p = 0.52 J (*a*), W_p = 2.6 J (*b*), W_p = 6.8 J (*c*) [56]

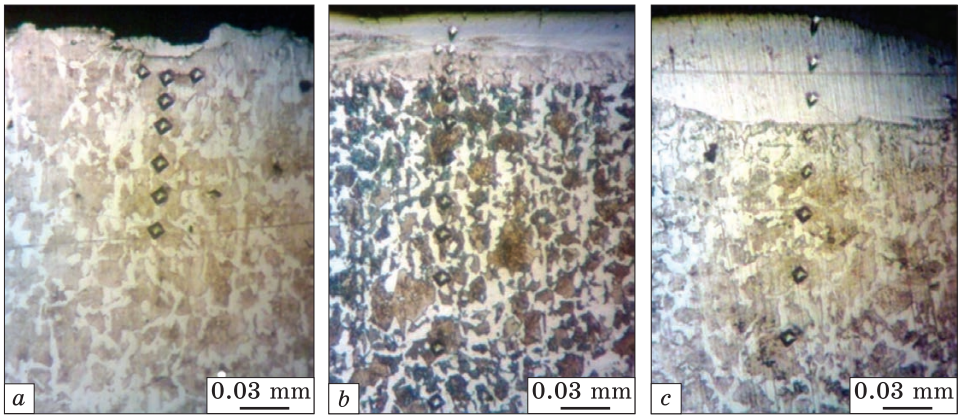

Fig. 6. Cross-sectional microstructure of steel 40 samples with aluminium coating: W_p = 0.52 J (*a*), W_p = 2.6 J (*b*), W_p = 6.8 J (*c*) [57]

The analysis of the measurement of the roughness of the steel sample 20 surface layer after the ESA process with aluminium has shown that the surface roughness increases with increasing the mode (Table 3): at W_p = 0.52 J, the roughness is R_a = 1.3; at W_p = 2.60 J, R_a = 3.3. A further increase in discharge energy up to 6.8 J is accompanied by a significant increase in the surface roughness: R_{max} = 58.305 μm, R_a = = 9.039 μm and R_z = 18.142 μm (Fig. 5).

The metallographic analysis of the aluminized coatings on steel 40 showed that, as well as on steel 20, the formation of the three (3) zones was observed (Fig. 6). It should be noted that, under the same conditions of the ESA process on steel 40, there are formed zones, which are larger in thickness (Table 1) and have the increased microhardness values (Fig. 7). Thus, at the ESA process of steel 40 with W_p = 2.60 J, the thickness of the 'white' layer is of 30–70 μm and the hardness (H_μ) of

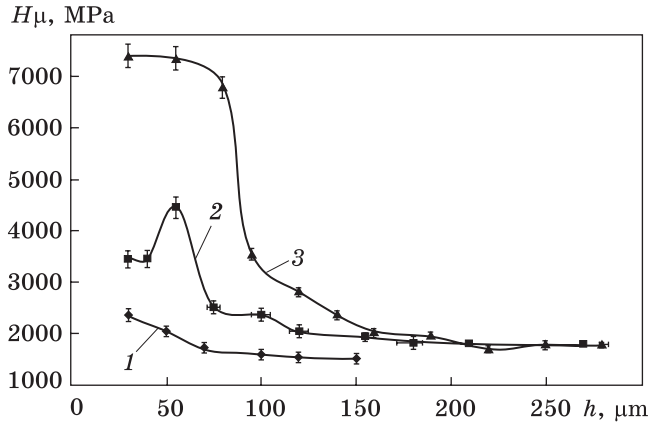

Fig. 7. Microhardness dependence on layer depth for steel 40 different processing modes: W_p = 0.52 J (*1*), W_p = 2.6 J (*2*), W_p = = 6.8 J (*3*) [57]

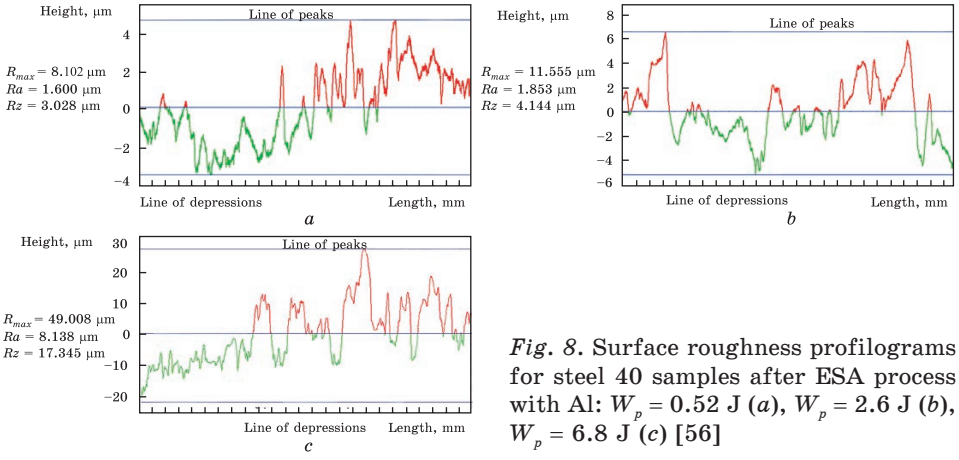

Fig. 8. Surface roughness profilograms for steel 40 samples after ESA process with Al: W_p = 0.52 J (*a*), W_p = 2.6 J (*b*), W_p = 6.8 J (*c*) [56]

3500 ± 50 MPa. The same for steel 20 is of 40–50 μm with H_μ = 2700 ± ± 70 MPa. As the discharge energy increases, the continuity of the 'white' layer increases, and that for the transition layer tends to 100% (Table 3).

With increasing the ESA modes, there is increasing the depth of the transition zone. At W_p = 0.52 J, it is not expressed, while at W_p = 2.6 J, it is of about 30–40 μm and is characterized by the increased hardness of about 4500 MPa.

The reason for such an increase in the hardness of the transition zone can be the phase transformations occurring therein when the steel is heated up to a temperature value above the critical one and cooled at an accelerated rate in the air. The section of incomplete recrystallization is clearly visible in the microstructure, which for steel 40 is determined by heating to the temperature range of 730–755 °C. The metal in this area is subject to partial recrystallization.

Along with the grains formed in the course of the recrystallization process, there are grains of the original metal. Despite cooling at the accelerated rate after the ESA process (in the air), in view of the low stability of the steel 40 supercooled austenite, the formation of a needle-type structure (martensite) does not occur, which fact, as a result of high hardness and brittleness, can lead to the formation of cracks. Therefore, it can be assumed that despite the increase in the hardness of the surface layer, its ability to small deformations remains. In addition, just as on steel 20, the formation of intermetallics, nitrides and oxides is possible in the surface layer, because the ESA process is carried out in the air, which event leads to a significant increase in the microhardness of the coating and the transition zone.

The analysis of the surface roughness measurements for steel 40 samples after the ESA process with aluminium showed that the surface roughness increases as soon as the ESA mode increases. At W_p = 0.52 J, the maximum surface roughness is $R_{\max}$ = 11.555 μm, and the average arithmetic values for R_a and R_z are of 1.853 and 4.144 μm, respectively (Fig. 8).

Thus, at the ESA process with an aluminium electrode of steel 20 and steel 40, with an increase in the discharge energy, such qualitative parameters of the surface layer as roughness, thickness, microhardness of the 'white' layer, and the transition zone increase (Table 3). The continuity of the 'white' layer at W_p = 0.52 J is low (of 50–60%), and with a further increase in the discharge energy, it increases and, at W_p = 6.8 J, is of up to 100%.

3.2. Influence of the Methods for Finishing Surface Treatment of the Parts after Aluminizing Thereof on the Quality of the Coatings

In Ref. [64], to reduce the roughness of the electroerosive coatings, it is proposed to carry out the so-called soft alloying with graphite as a final operation after the main alloying process. In this case, it is not a graphite layer that is formed, but some diffuse layer, and the cathode metal is ejected in the places where the pulses are applied, that is, the most protruding parts of the surface are sprayed. As a result, the combs are smoothed, and, therefore, the roughness of the surface is reduced.

In order to reduce the surface roughness after the ESA process with an aluminium electrode, the authors of the paper have proposed to carry out further processing with the same electrode (aluminium), but at lower modes [58]. At the same time, herein, an electric discharge flows between the top of the roughness protrusion and the aluminium electrode, destroying the top of the protrusion and decreasing the surface roughness. It was exposed [65] that such an ESA technology was effective.

Table 5 provides information on the productivity of the process at executing the ESA technology with carbon (graphite electrode) and alu-

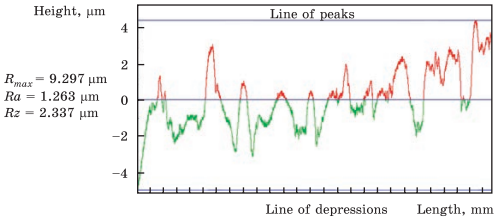

Fig. 9. Profilograms of the surface roughness of the sample made of steel 20 in the course of sequentially aluminizing by the ESA method with aluminium at the discharge energy values of W_p = 2.6 and 1.3 J [56]

Table 5. **Dependence of productivity for ESA process by carbon and aluminium of steel samples after their aluminization on the ESA discharge energy values [73]**

Discharge energy (W_p), J	0.52	1.3	2.6	4.8
Productivity, cm²/min				
ESA with aluminium	0.8–1.0	1.0–1.2	1.3–1.5	1.6–1.8
ESA with graphite electrode	0.5–0.7	0.7–1.0	1.0–1.2	1.2–1.5

minium relative the steel samples previously alloyed with aluminium, depending on the discharge energy.

Figure 9 shows the results of measuring the surface roughness values for the sample made of steel 20, which has been subjected to the aluminizing process by the ESA method, first at the discharge energy W_p = 2.6 J and the productivity of 1.8 cm²/min, and then at W_p = 1.3 J and the productivity of 0.8 cm²/min. As a result, the surface roughnesses are decreased as follow: R_{max} = 9.297, R_a = 1.263, and R_z = 2.337 μm.

3.3. Comparative Tests for Heat Resistance of the Aluminized Coatings

As far as is known, aluminized coatings provide iron-carbon alloys with increased heat resistance. In this regard, an urgent task is to study the heat resistance of aluminized coatings obtained by the ESA method. Steel 20 was used as a substrate, the ESA layers were obtained in two passes, first, with the discharge energy W_p = 2.6 J and the productivity of 1.8 cm²/min, and then, with the discharge energy W_p = 1.3 J and the productivity of 0.8 cm²/min. According to the results of the research, after such a treatment technology, the high-quality coatings (of 100% continuity) with low roughness characteristics were formed (Table 3, Fig. 5) [57].

For the comparative assessment of the heat resistance indices (Δg — mass loss per unit surface area of the samples being tested, mg/cm²), the samples made of steel 20 were tested after processing with the use of the classic aluminizing technology (aluminizing in molten aluminium described in detail in Ref. [66]) and without coating. The tests had been being carried out in the air at the temperature of 980 °C for 50 hours. The results

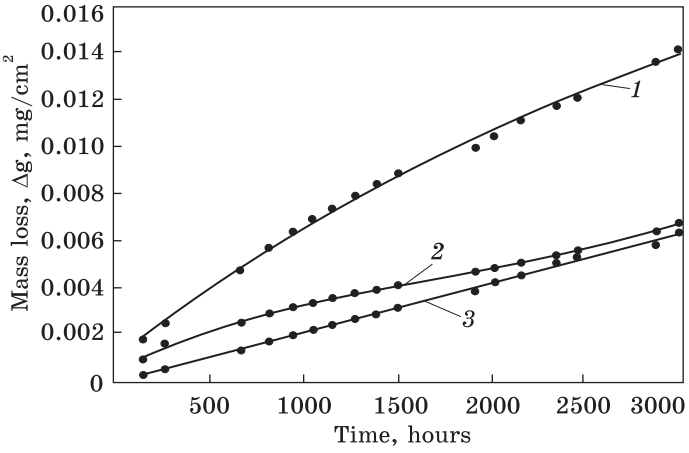

Fig. 10. Heat resistance of aluminized coatings on steel 20 (testing in the air at 980 °C, 50 h): *1* — without coating; *2* — aluminizing by the ESA method; *3* — aluminizing in molten Al [57]

showed that the obtained ESA coatings were characterized by high heat resistance values, even slightly higher than they are after the classical technology of aluminizing in molten aluminium. Such test results make it possible to recommend the technology of the ESA process with the use of an aluminium electrode for solving the technical problem of increasing steel oxidation resistance at elevated temperatures (Fig. 10).

After the heat resistance tests, the metallographic studies of the sample oxidation natures were carried out. The oxide inclusions could be observed at all the samples, and the samples without protective coatings were especially intensively oxidized (Fig. 11, *a*).

After liquidly aluminizing, in addition to the diffusion zone, on the aluminized surface layer, there is a zone of aluminium remained after the termination of the aluminizing process. This is evidenced by durometric studies.

After the heat resistance test (Fig. 11, *b*), there is observed the process of oxidation of the metal under the coating. This is evidenced by the presence of an oxide layer separating the surface layer and the base. Obviously, the similar nature of the destruction of the coating and, consequently, the oxidation of the base metal leads to a decrease in the mass of the samples in the course of the high-temperature tests (Fig. 10).

As for a sample with an aluminized coating obtained by the ESA method, a decrease in the thicknesses of the 'white' layer is observed (Fig. 11, *d*). Therefore, during the high-temperature tests, the destruction of the surface layer occurs, and in this event, the loss of mass is associated with a physicochemical process that mainly occurs in the surface layer, but not in the base metal. Moreover, despite the process of oxidation, the surface layer maintains increased hardness (Fig. 12).

Therefore, the aluminized coatings, which are obtained in molten aluminium and done by the ESA method, retain the increased hardness values

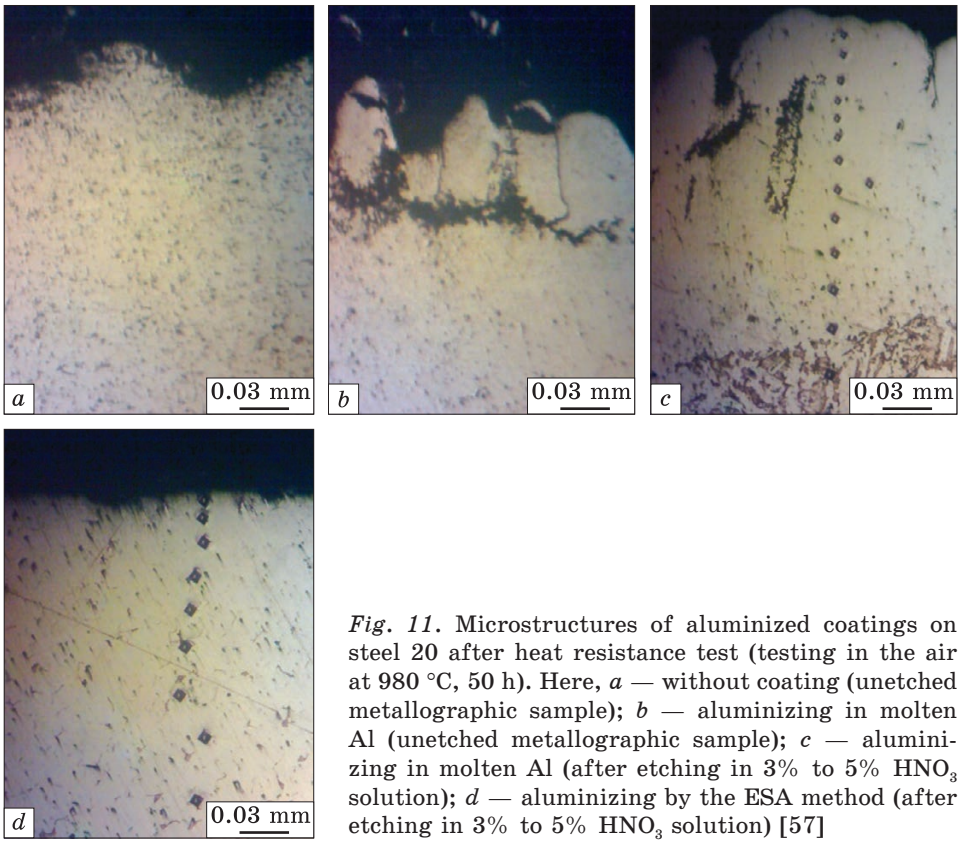

Fig. 11. Microstructures of aluminized coatings on steel 20 after heat resistance test (testing in the air at 980 °C, 50 h). Here, *a* — without coating (unetched metallographic sample); *b* — aluminizing in molten Al (unetched metallographic sample); *c* — aluminizing in molten Al (after etching in 3% to 5% HNO_3 solution); *d* — aluminizing by the ESA method (after etching in 3% to 5% HNO_3 solution) [57]

and protect the base metal from oxidation, which fact is evidenced by a smaller amount of oxides in the near-surface layer of the base metal (Fig. 11).

Thus, the analysis of the structural and phase formation features of the surface layers of carbon steels after aluminizing with the use of the ESA method showed that the structure of the layer consists of three zones: the 'white' layer, the diffusion zone, and the base metal. As the discharge energy increases, such qualitative parameters of the surface layer as thickness, microhardness of the 'white' layer and transition zone, and roughness increase. The continuity of the 'white' layer at $W_p = 0.52$ J is low (of 50–60%).With a further increase in the discharge energy, it increases and, at $W_p = 6.8$ J, it is of 100%. When the energy parameters of the ESA process are increased, the chemical and phase compositions of the layer change: at low discharge energies, a layer mainly consisting of α-Fe and aluminium oxides gets forming. With an increase in W_p, the layer starts consisting of intermetallics of iron and aluminium, as well as free aluminium. This event is confirmed by the data of local micro-x-ray spectral analysis.

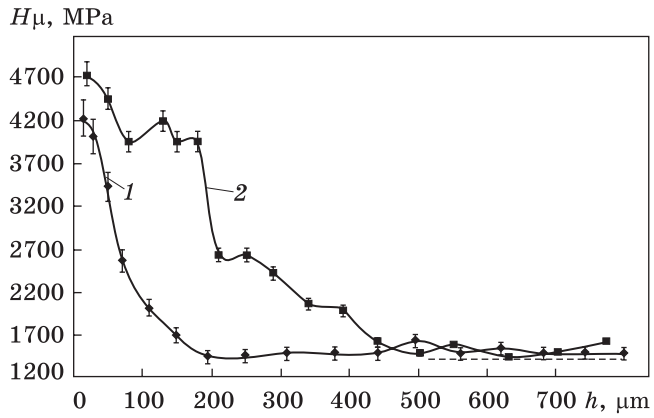

Fig. 12. Microhardness of aluminized coatings on steel 20 after heat resistance test (testing in the air at 980 °C, 50 hours): *1* — aluminizing by the ESA method; *2* — aluminizing in molten Al [57]

A comparative analysis of the substrate influence on the quality parameters of the surface layer has shown that when replacing steel 20 with steel 40, the thicknesses of the 'white' layer and the transition zone of steel 40 increase, namely, there increases the depth of its zone of increased hardness, the same concerns the value of its microhardness. Surface roughness practically does not change.

For practical application, it is possible to recommend the process of aluminizing by the ESA method with the use of the modes (discharge energy with $W_p = 4.6–6.8$ J and productivity of 2.0–3.0 cm^2/min), which ensure the formation of the 'white' layer of 70–130 microns thick, microhardness of 5 000–7 500 MPa, roughness (R_a) of 6–9 microns and continuity of 95–100%.

In order to reduce the roughness of the surface layer and to obtain the continuous coatings, it is recommended to perform ESA process with the same electrode (aluminium), but at the lower modes.

The comparative studies of heat resistances of the aluminized coatings obtained by the classical technology (in molten aluminium) and those done by the ESA process with an aluminium electrode have shown that the electrospark coatings are characterized by high heat resistance. The conducted metallographic analysis of the nature of the oxidation of the sample after the heat resistance test has shown that after the test, the base metal is oxidized, which event is evidenced by the presence of oxides in the surface layer. The samples without protective coatings oxidize especially intensively. Obtained in molten aluminium and by the ESA method, the aluminized coatings retain the increased hardness values protect the base metal from oxidation, as evidenced by the lower content of oxides in the surface layer of the base metal and sufficient hardness of the coating. The results of the study make it possible to recommend the ESA technology with an aluminium electrode to increase the resistance of steel to oxidation at elevated temperatures.

3.4. Quality Parameters of Multicomponent Composite Coatings

3.4.1. Al–C–S Coatings Obtained via the ESA Methods

Complex Al–C–S coatings were obtained by the ESA method according to the technology presented in Table 6.

The microstructural analysis of the samples has shown that in the surface layer, the formation of individual depressions with a depth of up to 150 μm is observed. As shown in [68], when an electric-spark discharge passes through a metal, a depression of a crater type is formed; the depth and diameter of such a depression depend on the parameters of the electric spark effect. The spark discharge is accompanied by the heat generation; the rate of temperature increase is of up to 10^5 °C/sec, which is typical only for explosive processes [69]. According to paper [70], about 25% of the metal volume in the electroerosive depressions reaches the boiling point, and the instantaneous pressures on the surface reach hundreds of thousands atmospheres.

On the sample of steel 20, the three zones have been being distinguished in the area of the depression of the crater type (Fig. 13).

The first is a reflowing and poorly etched zone. During the ESA process, the metal in this zone is in a liquid state. It consists of columnar crystals. The high rate of crystallization determines the anisotropy

Table 6. **Technology for obtaining complex Al–C–S coatings [73]**

Viscous substance composition	Alloying electrode (anode)
33.3% S + 56% Al (mass.%)	graphite

Table 7. **Qualitative parameters of surface layers of Al–C–S system obtained by the ESA method on steel 20 and steel 40 [56]**

Discharge energy, J	Thickness of 'white' layer, μm	Microhardness of 'white' layer, MPa	Roughness, μm			Continuity of 'white' layer,%
			R_a	R_z	R_{max}	
Steel 20						
0.52	150	9300 ± 50	2.1	3.9	8.9	90
2.60	110	9200 ± 70	4.2	8.7	30.2	80
6.8	till 60	9000 ± 50	8.5	10.2	62.4	50
In stages 6.8 and 2.6	till 60	9000 ± 50	4.3	8.4	32.3	70
In stages 6.8; 2.6 and 0.52	till 60	9000 ± 50	2.6	4.4	11.5	80
Steel 40						
0.52	till 180	9500 ± 50	1.9	3.8	8.7	90
2.60	till 130	9300 ± 50	3.9	8.5	15.3	80
6.8	till 80	9100 ± 50	7.8	11.3	58.1	60

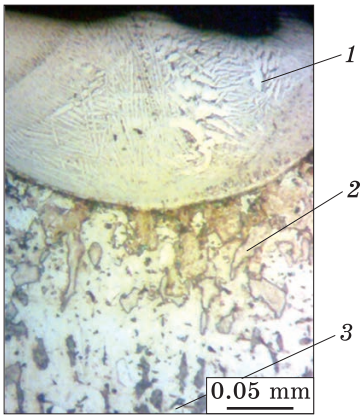

Fig. 13. Microstructure of steel 20 sample: *1*, *2*, *3* are zones in the region of depression of crater type (electrode is graphite, W_p = 6.8 J, surface of steel 20 sample before ESA process is covered with a viscous substance composition containing 33.3% of sulphur and 56% of Al powder) [67]

of the crystal growth, namely, the accelerated growth of the main axes of dendrites oriented in the direction of heat removal. On the side surface, the thickness of the layer of the columnar crystals increases from the bottom to the exit of the depression [71, 72].

The second is a transition zone, which is adjacent to the first and consists of the grains of complex shapes. This is the zone of thermal influence. The third is the original metal zone, which is adjacent to the first two ones and has an original structure.

There has been studied the effect of the ESA modes on the quality parameters of Al–C–S coatings.

The microstructural analysis of Al–C–S coatings on steel 20 showed that (Fig. 14, *a*) the 'white' layer was formed on the surface; after it, the diffusion zone and the base metal were observed. It should also be noted that at processing steel 20 with the use of the ESA method by graphite, the continuity and the thickness of the 'white' layer was of 50% and 60 μm, respectively (at W_p = 6.8 J). In turn, the microhardness on the surface was 9000 MPa (Fig. 14, *b* and Table 7. In Ref. [68], it was shown that

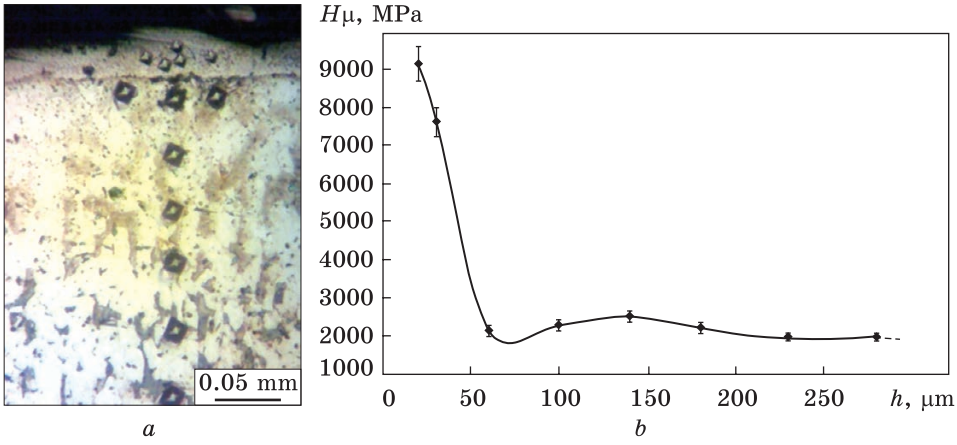

Fig. 14. Microstructure (*a*) and distribution of microhardness in the surface layer (*b*) of steel 20 sample after processing with the use of the ESA method by a graphite electrode (W_p = 6.8 J) [56]

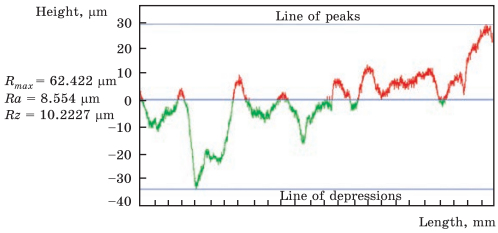

Fig. 15. Profilograms of steel 20 sample surface layers comprising 33.3% S + + 56% Al (wt.%) after processing with the use of the ESA method by graphite electrode at W_p = = 6.8 J) [67]

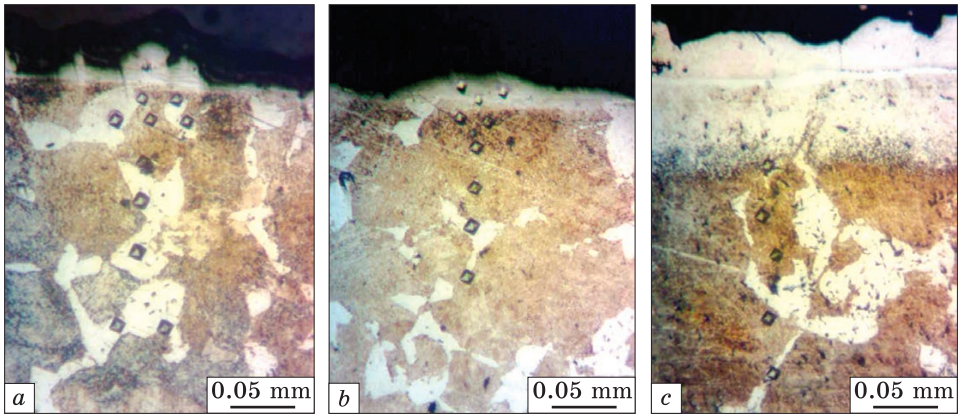

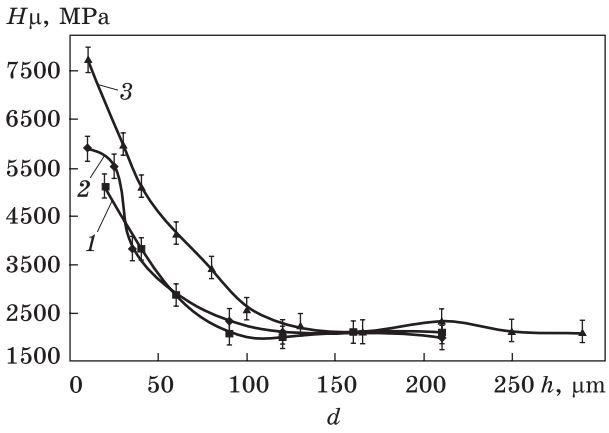

Fig. 16. Microstructures (*a*–*c*) and distribution of microhardness in the surface layer (*d*) of 38Kh2MUA (41CrAlMo7) steel samples after saturating thereof with S, Al, and C by the ESA method. Here, (*a*–*c*) W_p = 0.13 J (*a*), W_p = 0.52 J (*b*), W_p = 4.9 J (*c*); (*d*) W_p = 0.13 J (*1*), W_p = 0.52 J (*2*), W_p = 4.9 J (*3*) [73]

in the course of the electrospark treatment of the iron-based alloys, there was a significant decrease in the size of the substructure blocks, an increase in the defect concentration, and an increase in the number of the microdistortions of the thermal influence zone. Such changes in the microstructure and substructure of the steel led to a noticeable increase in the microhardness of the 'white' layer (Fig. 14). The atmospheric elements (nitrogen, oxygen) can play a certain role in increasing the hardness. While passing under the action of electric discharges into an active state, those can interact with the surface layers and strengthen the material.

The presence of sulphur in the solid substance contributes to the sulphidizing process. Table 8 shows the change in the sulphur content by depth from the surface of steel 20 after the ESA process with the discharge energy of 6.80 J. Thus, the amount of sulphur is maximum on the surface, and it has been decreasing with distance from the surface.

It should be noted that at simultaneously saturating steel with carbon, sulphur and aluminium by the ESA method, with a significant increase in the discharge energy (from 0.52 to 6.8 J) there is an increase in surface roughness and a decrease in the continuity of the coating (Table 7). Figure 15 shows the sample surface profilograms after processing with the use of the ESA method.

A study of simultaneously saturating 38Kh2MUA (41CrAlMo7) steel with carbon, sulphur and aluminium by the ESA method with the use of a graphite electrode at different modes has been carried out.

The metallographic analysis has shown that the coatings obtained at W_p = 0.13 J and 0.52 J consist of three areas (Fig. 16): (1) 'white' layer, (2) transition zone, (3) base metal.

However, along with an increase in the discharge energy of up to 4.9 J, a sublayer of up to 10 μm thick has been being formed between the 'white' layer and the transition zone (Fig. 16, *c*).

In addition, along with an increase in the discharge energy, the thickness of the 'white' layer and its continuity have been increasing (Table 9). Thus, at W_p = 0.13 J and W_p = 4.9 J, the thickness of the 'white' layer is of 10 μm and 70 μm; the continuity is of 60% and 100%, respectively.

The durometric studies have shown that along with increasing the discharge energy, the microhardness of the 'white' layer has been in-

Table 8. **Sulphur content in steel 20 surface layer, while processing by the ESA method at simultaneously saturating steel with carbon, sulphur and aluminium [56]**

Distance from the surface, μm	20	40	60	80	100	120	140	160	180
Sulphur content, %	0.21	0.15	0.12	0.09	0.08	0.05	0.05	0.03	0.03

Table 9. **Qualitative parameters of surface layers at simultaneously saturating of 38KhX2MUA (41CrAlMo7) steel with carbon, sulphur, and aluminium with the use of ESA method [67]**

Discharge energy, J	Thickness of 'white' layer, μm	Microhardness of 'white' layer, MPa	Roughness, μm			Continuity of 'white' layer,%
			R_a	R_z	R_{max}	
0.13	10	5126	0.8	2.1	6.5	60
0.52	30	5890	2.3	4.4	15.1	90
4.9	70	7721	8.2	18.3	47.3	100

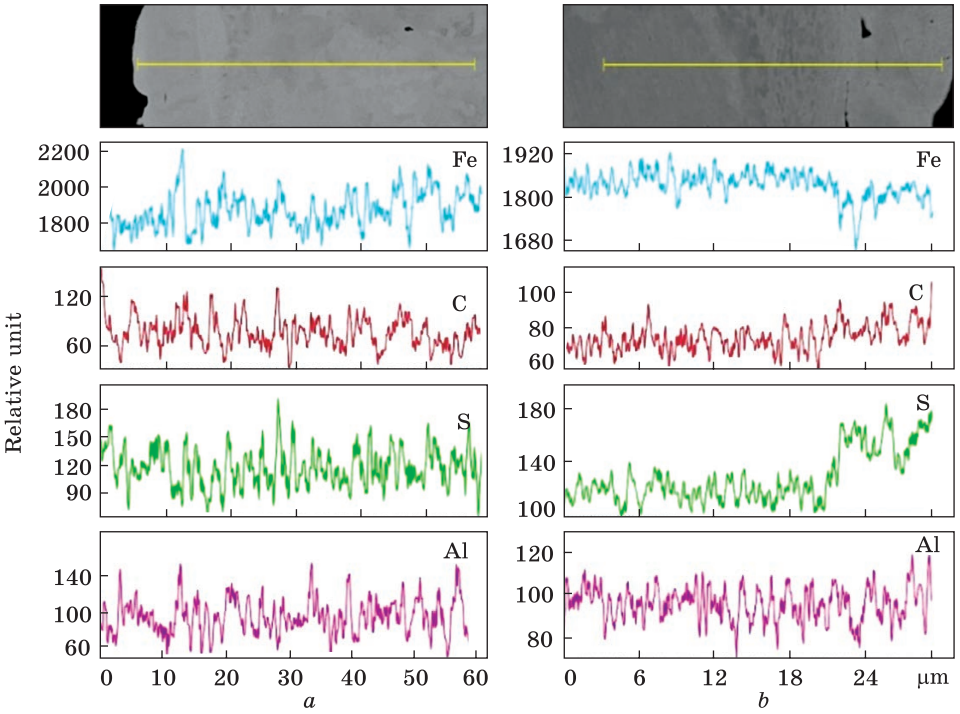

Fig. 17. Distribution of elements in the Al–C–S coating obtained with the use of ESA method: W_p = 0.13 J (*a*); W_p = 4.9 J (*b*) [73]

creasing. Thus, at the discharge energy of W_p = 0.13 J, H_μ = 5126 MPa, and at W_p = 4.9 J, H_μ = 7721 MPa (Fig. 16, *d*).

The discharge energy, whereat the ESA process takes place, affects the distribution of the elements in the resulting coating. The analysis of Fig. 17 picture disclosed that, with an increase in the discharge energy on the surface of the coatings, a decrease in the mount of sulphur is observed, which is apparently associated with the burning out of sulphur during the flow of a pulsed discharge during the ESA process.

Thus, the peculiarities of the Al–C–S coating structure formation obtained by the ESA method have been investigated. It has been shown that the formation of separate depressions of up to 150 μm in depth is observed in the surface layer. On the steel 20 sample, the three zones have been being distinguished in the area of the depression crater. The first is a reflowing and poorly etched zone. In the course of the ESA process, the metal in this zone is in a liquid state. The second is a transition zone, which is adjacent to the first and consists of the grains of complex shapes. This is a zone of thermal influence. The third is the original metal zone, which is adjacent to the first two ones and has an original structure. The effect of the ESA process modes on the quality parame-

ters of the Al–C–S coatings has been studied. With a significant increase in the discharge energy (from 0.52 to 6.8 J), there is an increase in the surface roughness and a decrease in the continuity of the coating.

The microstructural analysis of Al–C–S coatings on steel 20 showed that the continuity and thickness of the 'white' layer was 50% and 60 μm, respectively (at W_p = 6.8 J). In turn, the microhardness on the surface is of 9000 MPa. The presence of sulphur in the solid substance contributes to the occurrence of the sulphidizing process. In this event, the amount of sulphur is maximum on the surface and decreases with distance from the surface. There has been carried out the investigation of the process for simultaneously saturating 38KhX2MUA (41CrAlMo7) steel with carbon, sulphur and aluminium by the ESA method with a graphite electrode at different modes. The metallographic analysis has shown that the coatings obtained at W_p = 0.13 J and 0.52 J consist of three (3) zones: the 'white' layer, the transition zone and the base metal zone. However, with an increase in discharge energy of up to 4.9 J, a sublayer with a thickness of up to 10 μm is formed between the 'white' layer and the transition zone. In addition, with an increase in the discharge energy, the thickness of the 'white' layer, its microhardness and continuity increase. Thus, at W_p = 0.13 J and W_p = 4.9 J, the thickness of the 'white' layer is of 10 and 70 μm, H_μ = 5126 MPa and H_μ = 7721 MPa, the continuity is of 60 and 100%, respectively. The x-ray microspectral analysis has shown that the sulphur content is maximum on the surface and decreases sharply deeper into the metal.

3.4.2. Al–C–B Coating Obtained from the ESA Methods with Aluminium Electrode

The research results indicate that the microstructure of Al–C–B coatings consists of several areas, the number and parameters of which are determined by the energy modes of the ESA process (Fig. 18).

At the relatively low discharge energies of 0.13 J and 0.55 J, the obtained layers consist each of three areas, namely, the upper 'white' strengthened layer, the diffusion zone, and the base metal that is, steel 40 of a ferrite–pearlite structure (Fig. 18, *a, b*). In this case, a value of the 'white' layer for the above modes is of 15–20 μm (Table 10). An increase in the discharge energy of up to 4.9 J results in changing the number of the areas and their structures (Fig. 18, *c*). Those are as follows: the upper layer of a dendritic structure becomes of up to 60 μm, there occurs an interlayer of up to 20 μm, the diffusion zone, which is characterized by crushed structural components and in this connection, has an increased etch ability in a reagent, and the base metal.

The durometric studies showed that with increasing energy impact during the ESA process, the microhardness of both the upper streng-

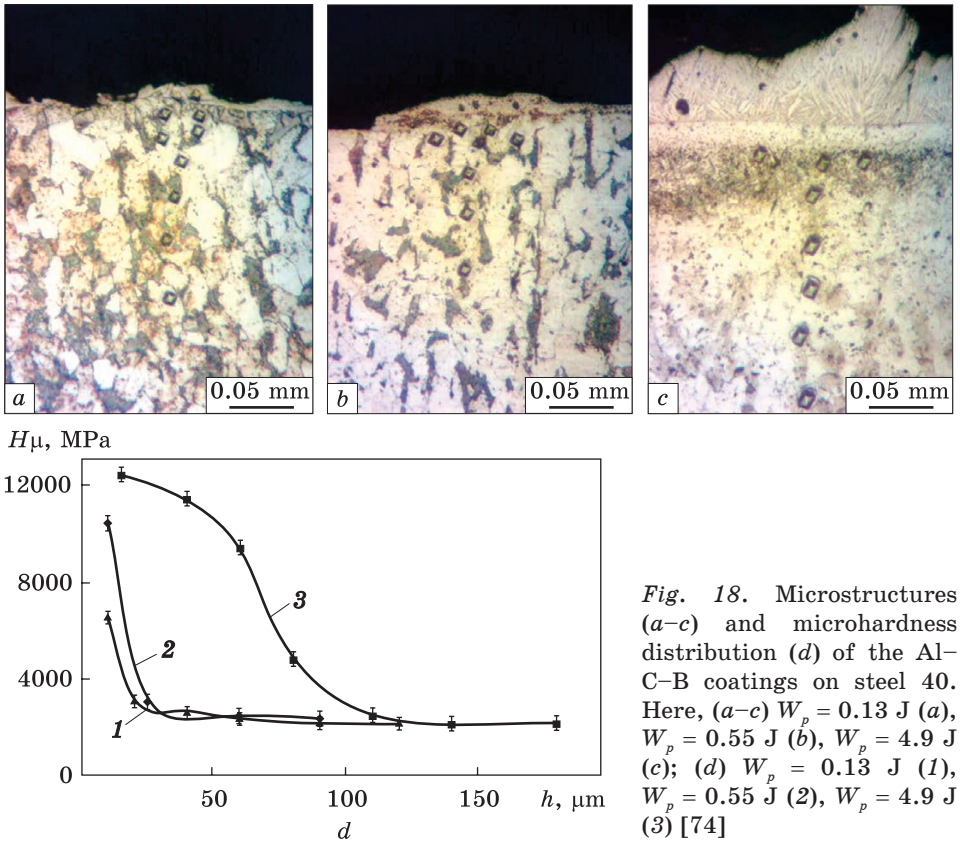

Fig. 18. Microstructures (*a*–*c*) and microhardness distribution (*d*) of the Al–C–B coatings on steel 40. Here, (*a*–*c*) W_p = 0.13 J (*a*), W_p = 0.55 J (*b*), W_p = 4.9 J (*c*); (*d*) W_p = 0.13 J (*1*), W_p = 0.55 J (*2*), W_p = 4.9 J (*3*) [74]

Table 10. **Qualitative parameters of Al–C–B coatings obtained by the ESA method (here, *S* is a layer continuity) [73, 74]**

Discharge energy, J	Roughness, μm			Strengthened layer		
	R_a	R_z	R_{max}	$H_μ$, МПа	*h*, μm	*S*, %
Steel 20						
0.13	1.1	2.7	7.2	5474	20	60
0.55	2.9	4.1	16.3	10196	30	80
4.9	8.9	18.7	46.1	11345	75	98
Steel 40						
0.13	1.2	2.9	7.4	6487	15	55
0.55	2.9	4.5	17.3	10351	20	75
4.9	9.3	19.5	48.2	12350	60	95

thened layer and the diffusion zone has been increasing (Fig. 18, *d*). Thus, at W_p = 0.13 J, $H_μ$ = 6487 MPa, and at W_p = 4.9 J, $H_μ$ = 12350 MPa (Table 10).

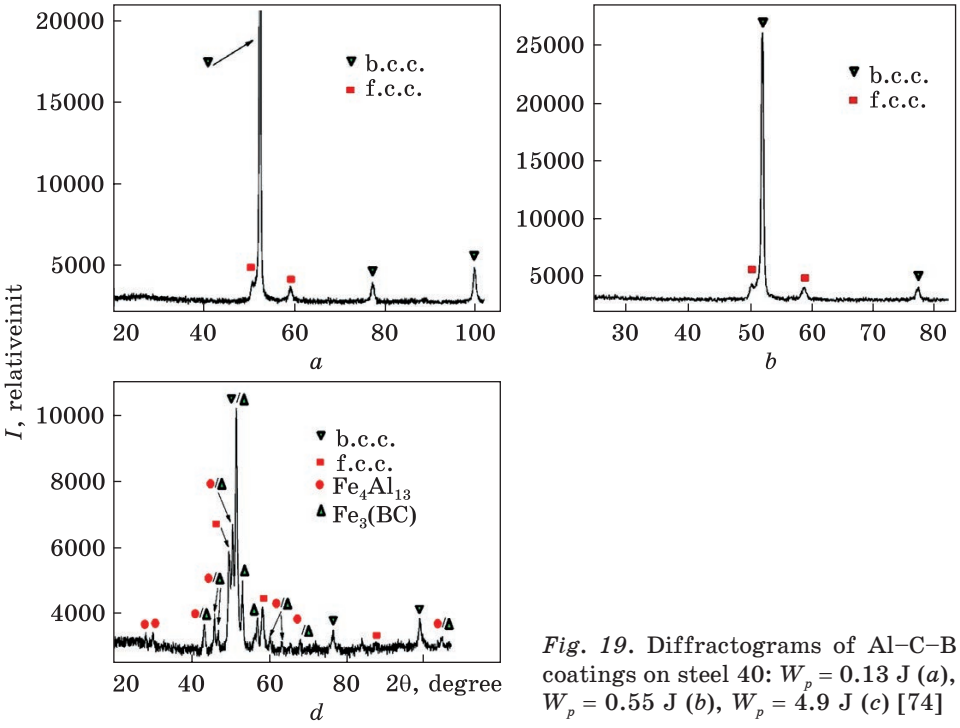

Fig. 19. Diffractograms of Al–C–B coatings on steel 40: W_p = 0.13 J (*a*), W_p = 0.55 J (*b*), W_p = 4.9 J (*c*) [74]

Table 11. **Crystal lattice parameters and quantitative phase analysis of Al–C–B coatings on steel 40 [74]**

Discharge energy, J	Phase	Lattice periods, nm	Phase content, (wt.%)
0.13	f.c.c. solid solution	36.189	8.25
	b.c.c. solid solution	28.651	91.75
0.55	f.c.c. solid solution	36.189	8.31
	b.c.c. solid solution	28.651	91.69
4.9	Fe_4Al_{13}	a = 153.920 b = 81.779 c = 124.914 β = 107.3709	9.46
	$Fe_3(CB)$	a = 50.81 b = 67.79 c = 45.170	43.43
	f.c.c. solid solution	a = 36.209	14.12
	b.c.c. solid solution	a = 28.699	32.88

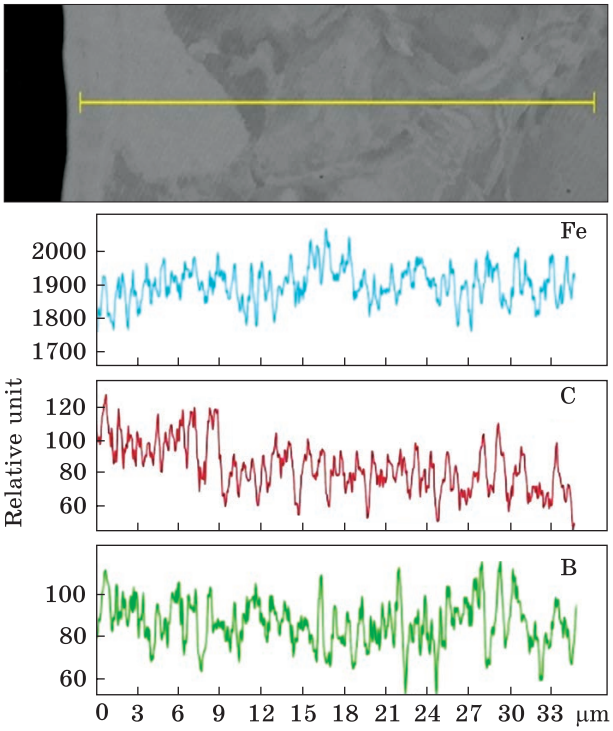

Fig. 20. Distribution of Fe, C, and B in Al–C–B coatings on steel 40 (W_p = 0.13 J) [73]

The results of the x-ray structural analysis indicate that at relatively low discharge energies (0.13 and 0.55 J), the phase composition of the coatings is represented by the solid solutions of b.c.c. and f.c.c. (Fig. 19), with the parameters a = 28.651 nm and a = 36.189 nm, respectively (Table 11). Therefore, it can be assumed that, while simultaneously saturating steel 40 with Al, C and B by the ESA method, because of mixing the base material with a viscose substance containing aluminium powder and the material of the graphite electrode, there occurs the process of alloying the b.c.c. solid solution, and as a result, its parameter increases. In addition, accelerated cooling after the ESA process leads to the formation of thermal stresses causing an additional increase in the parameter a and the microhardness of the coating.

In addition to the b.c.c. and f.c.c. solid solutions with the crystal lattice parameters changed to a greater extent (Table 11), the coatings obtained at W_p = 4.9 J are characterized by the presence of the intermetallics Fe_4Al_{13} and the alloyed cementite $Fe_3(CB)$. The formation of these phases contributes to a significant strengthening and increase of the microhardness of the surface layer up to 12350 MPa (Table 10).

The x-ray microspectral analysis of the resulting coatings shows that the surface layers have been being saturated with aluminium, boron, and carbon in the course of electrospark alloying. While increasing the discharge energy, the diffusion zone has been increasing. Thus, at the ESA process with W_p = 0.13 J of steel 40, the diffusion zone is of 10–15 μm (Fig. 20).

At replacing the substrate made of steel 40 by that of steel 20, because of the ESA process, an increase in the thickness of the surface

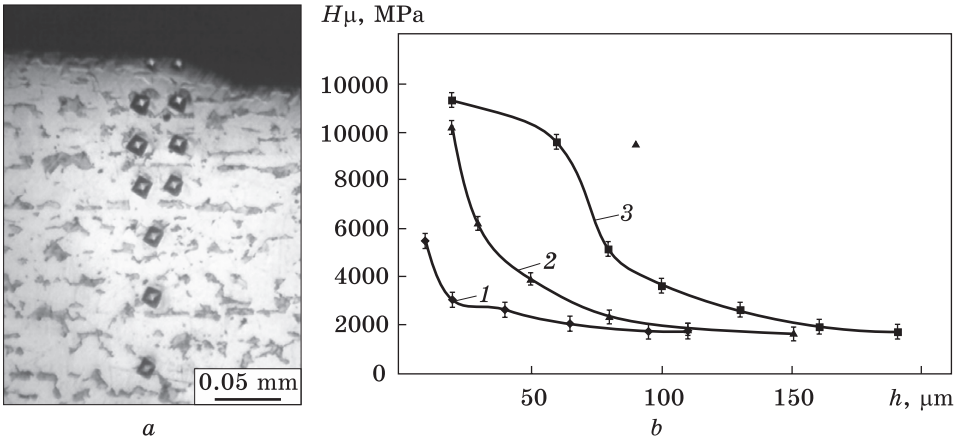

Fig. 21. Microstructures (*a*, *c*) and distributions of Al–C–B coating microhardness values (*b*) on steel 20: (*a*, *c*) W_p = 0.55 J (*a*), W_p = 0.55 J (*c*); (*b*) W_p = 0.13 J (*1*), W_p = 0.55 J (*2*), W_p = 4.9 J (*3*) [73]

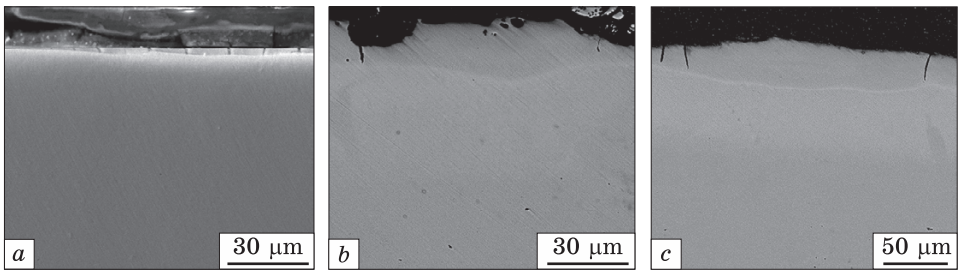

Fig. 22. Structures of surface Al–C–B coatings obtained by the ESA method on steel 20, where W_p = 0.13 J (*a*), W_p = 0.55 J (*b*), and W_p = 4.9 J (*c*) [73]

layer is observed with a slight decrease in the microhardness thereof (Fig. 21).

Figure 22 shows the results of the electron microscopic studies of the Al–C–B coatings on steel 20. At W_p = 0.13 J, the thin and discontinuous layers are formed. With increasing the discharge energy values,

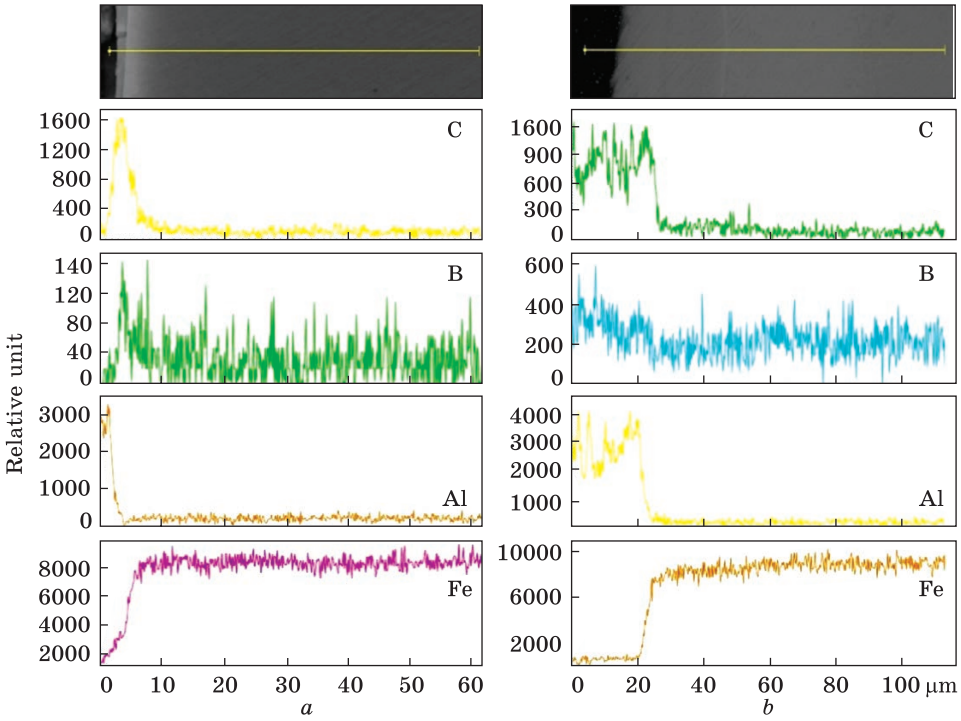

Fig. 23. Distribution of elements in Al–C–B coatings obtained by the ESA method with a graphite electrode on steel 20, where W_p = 0.13 J (*a*) and W_p = 4.9 J (*b*) [74]

the thicknesses of the coatings and their continuity values have been increasing. In addition, it should be noted that with increasing the discharge energy value, the diffusion zone of Al, C, and B has been increasing. Thus, at W_p = 0.13 J, this zone is of 5–7 μm, while at W_p = 4.9 J, it is of 23–25 μm (Fig. 23). Carbon and aluminium diffuse to a greater extent in depth from the surface.

Thus, the microstructural analysis of the Al–C–B coating on steel 40 showed that the surface layer consists of several areas, the number and parameters of which are determined by the energy modes of the ESA process. At discharge energies of 0.13 and 0.55 J, the layers consist each of three areas, namely, the upper 'white' strengthened layer, the diffusion zone and the base metal that is, steel 40 of a ferrite–pearlite structure. In this case, the size of the 'white' layer for these modes is of 15–20 μm.

An increase in the discharge energy up to 4.9 J results in changing the number of the areas and their structures. They are as follows: the upper layer of a dendritic structure becomes of up to 60 μm, there occurs an interlayer of up to 20 μm, the diffusion zone, which is characterized by crushed structural components and in this connection, has an

increased etch ability in a reagent, and the base metal. Durometric studies have shown that with increasing energy impact in the course of the ESA process, the microhardness of both the upper strengthened layer and the diffusion zone have been increasing: at W_p = 0.13J, H_μ = = 6487 MPa, and at W_p = 4.9 J, it is of 12350 MPa.

The results of the x-ray structural analysis have indicated that at discharge energies of 0.13 J and 0.55 J, the phase compositions of the coatings are represented by the solid solutions of b.c.c. and f.c.c. with the parameters a = 28.651 nm and 36.189 nm, respectively. The coatings obtained at W_p = 4.9 J are characterized by the presence of the Fe_4Al_{13} intermetallics and alloyed Fe_3(CB) cementite, in addition to the b.c.c. and f.c.c. solid solutions with the crystal lattice parameters changed to a greater extent. The formation of the above phases contributes to significantly strengthening and increasing in the microhardness of the surface layer up to 12350 MPa.

The x-ray microspectral analysis of the resulting coatings showed that the surface layers had been being saturated with aluminium, boron, and carbon during the process of electrospark alloying. At increasing the discharge energy, the diffusion zone has been increasing: at processing steel 40 with the use of the ESA method at W_p = 0.13 J, the diffusion zone is of 10–15 μm. When replacing the substrate made of steel 40 by that of steel 20, owing to the use of the ESA method, there is observed an increase in the thickness of the surface layer with a slight decrease in the microhardness thereof. At W_p = 0.13 J, the thin and non-continuous layers are formed. At increasing the discharge energy, the thicknesses of the coatings and their continuity values have been increasing. It should be noted that, at increasing of the discharge energy, the diffusion zone of Al, C, and B has been increasing: at W_p = 0.13 J, this zone is of 5–7 μm, while at W_p = 4.9 J, it is of 23–25 μm. Carbon and aluminium diffuse more in depth from the surface.

4. Summary and Conclusions

The unique features of structure formation in the course of aluminizing steel 20 and steel 40 under various ESA modes are considered. It is shown that the layer structure consists of three areas: the 'white' layer, the diffusion zone, and the base metal.

It has been established that with increasing discharge energy, the parameters of surface layer quality such as thickness, microhardness of the 'white' layer and transition zone and roughness increase. The continuity of the 'white' layer at W_p = 0.52 J is low (of 50–60%), with a subsequent increase in the discharge energy, it increases and, at W_p = 6.8 J, it is of 100%.

It has been determined that hardening the ESA process leads to a change in the chemical and phase compositions of the layer: at low dis-

charge energies, a layer is formed, consisting mainly of α-Fe and aluminium oxides. With an increase in W_p value, the layer consists of iron and aluminium intermetallic compounds, as well as free aluminium, which fact is confirmed by the data of the local x-ray microanalysis.

A comparative analysis, which had been being conducted to determine the substrate influence on the quality characteristics of the surface layer while aluminizing thereof by the ESA method, showed that when replacing steel 20 with steel 40, the thickness of the 'white' layer and transition zone (*i.e.* the depth of the zone of increased hardness as well as the value of its microhardness) increased. The surface roughness remained virtually unchanged.

For practical application, there should be recommended the process of aluminizing by the ESA method performed at the modes (the discharge energy W_p = 4.6–6.8 J and the productivity of 2.0–3.0 cm^2/min), which provide the formation of the white layer with the thickness of 70–130 μm, the microhardness of 5000–7500 MPa, the roughness (R_a) of 6–9 μm, and the continuity of 95–100%.

To increase the thickness of the layer aluminized by the ESA method, a viscous substance containing aluminium powder, for example, that consisting of 33.3% S + 56% Al (mass.%), is applied on the aluminized surface of the steel, and without waiting for it to dry, the ESA process is performed with an aluminium electrode. In this case, the coating continuity is of 100%, the layer thickness is of up to 200 μm, and the microhardness is of 4500 MPa. The presence of sulphur in the viscous substance contributes to the performance of the sulphidizing process.

Replacing the aluminium electrode with graphite (carbon) leads to a decrease in the thickness and continuity of the 'white' layer, respectively, to 50 μm and 30% thereof. In turn, the microhardness on the surface increases up to 9000 MPa.

The addition of 0.7 boron to the viscous substance leads to an increase in the thickness and continuity of the 'white' layer, respectively, up to 60 μm and 70%. In turn, the microhardness on the surface increases up to 12000 MPa.

In order to reduce the roughness of the surface layer and obtain continuous coatings, it is recommended to carry out the ESA process with an aluminium electrode, but at lower modes.

REFERENCES

1. V. Tarelnyk, V. Martsynkovskyy, O. Gaponova, Ie. Konoplianchenko, M. Dovzyk, N. Tarelnyk, and S. Gorovoy, *IOP Conf. Ser.: Mater. Sci. Eng.*, **233**: 012049 (2017); https://doi.org/10.1088/1757899X/233/1/012049
2. V. Martsynkovskyy, V. Tarelnyk, V. Martsynkovskyy, Ie. Konoplianchenko, A. Zhukov, P. Kurp, P. Furmańczyk, and N. Tarelnyk, *Electromachinihg-18: American Institute of Physics Conf. Proceedings* (May 9–11, 2018, Bydgoszcz), p. 020017; https://aip.scitation.org/doi/abs/10.1063/1.5056280

3. V. Tarelnyk, Ie. Konoplianchenko, V. Martsynkovskyy, A. Zhukov, and P. Kurp, *Advances in Design, Simulation and Manufacturing. DSMIE-2018. Lecture Notes in Mechanical Engineering,* (Cham: Springer: 2019), 382; https://doi.org/10.1007/978-3-319-93587-4_40
4. V.B. Tarelnik, V.S. Martsinkovskii, and A.N. Zhukov, *Chemical Petroleum Engineering*, **53**, Nos. 3–4: 266 (2017); https://doi.org/10.1007/s10556-017-0333-7
5. V.B. Tarelnik, V.S. Martsinkovskii, and A.N. Zhukov, *Chemical Petroleum Engineering*, **53**, Nos. 5–6: 385 (2017); https://doi.org/10.1007/s10556-017-0351-5
6. T.V. Mosina, *Novye Ogneupory (New Refractories)*, **9**: 61 (2013) (in Russian); https://doi.org/10.17073/1683-4518-2013-9-61-64
7. P. Rohatgi, *JOM*, **43**: 10 (1991); https://doi.org/10.1007/BF03220538
8. A. Zahorulko, C. Kundera, and S. Hudkov, *IOP Conference Series: Materials Science and Engineering*, **233** (1): 012039 (2017); https://doi.org/10.1088/1757-899X/233/1/012039
9. I.P. Shatskyi, V.V. Perepichka, and L.Ya. Ropyak, *Metallofiz. Noveishie Tekhnol.*, **42**, No. 1: 69 (2020) (in Ukrainian); https://doi.org/10.15407/mfint.42.01.0069
10. M.S. Storozhenko, A.P. Umanskii, A.E. Terentiev, and I.M. Zakiev, *Powder Metall. Met. Ceram.*, **56**, Nos. 1–2: 60 (2017); https://doi.org/10.1007/s11106-017-9847-y
11. O. Umanskyi, M. Storozhenko, G. Baglyuk, O. Melnyk, V. Brazhevsky, O. Chernyshov, O. Terentiev, Yu. Gubin, O Kostenko, and I. Martsenyuk, *Powder Metall. Met. Ceram.*, **59**, Nos. 7–8: 434 (2020); https://doi.org/10.1007/s11106-020-00177-y
12. M. Bembenek, P. Prysyazhnyuk, T. Shihab, R. Machnik, O. Ivanov, and L. Ropyak, *Materials*, **15**, No. 14: 5074 (2022); https://doi.org/10.3390/ma15145074
13. B.O. Trembach, M.G. Sukov, V.A. Vynar, I.O. Trembach, V.V. Subbotina, O.Yu. Rebrov, O.M. Rebrova, and V.I. Zakiev, *Metallofiz. Noveishie Tekhnol.*, **44**, No. 4: 493 (2022); https://doi.org/10.15407/mfint.44.04.0493
14. L. Ropyak, I. Schuliar, and O. Bohachenko, *Eastern-European Journal of Enterprise Technologies*, **1**, No. 5 (79): 53 (2016) (in Ukrainian); https://doi.org/10.15587/1729-4061.2016.59850
15. I. Ivasenko, V. Posuvailo, H. Veselivska, and V. Vynar, *International Scientific and Technical Conference on Computer Sciences and Information Technologies*, **2**: 9321900 (2020); https://doi.org/10.1109/CSIT49958.2020.9321900
16. M. Bembenek, M. Makoviichuk, I. Shatskyi, L. Ropyak, I. Pritula, L. Gryn, and V. Belyakovskyi, *Sensors*, **22**, No. 21: 8105 (2022); https://doi.org/10.3390/s22218105
17. M.M. Student, V.M. Dovhunyk V.M., Posuvailo, I.V. Koval'chuk, and V.M. Hvozdets'kyi, *Materials Science*, **53**, No. 3: 359 (2017); https://doi.org/10.1007/s11003-017-0083-x
18. O. Bazaluk, O. Dubei, L. Ropyak, M. Shovkoplias, T. Pryhorovska, and V. Lozynskyi, *Energies*, **15**, No. 1: 83, (2022); https://doi.org/10.3390/en15010083
19. M. Bembenek, T. Mandziy, I. Ivasenko, O. Berehulyak, R. Vorobel, Z. Slobodyan,

and L. Ropyak, *Sensors*, **22**, No. 19: 7600 (2022); https://doi.org/10.3390/s22197600
20. F.A.P. Fernandes, S.C. Heck, R.G. Pereira, and A. Lombardi-Neto, *Journal of Achievements in Materials and Manufacturing Engineering*, **40**, No. 2: 175 (2010).
21. Shu-Hung Yeh, Liu-Ho Chiu, and Heng Chang, *Engineering, Scientific Research Publishing*, **9**, No. 3: 942 (2011).
22. S. Ben Slima, *Materials Sciences and Applications, Scientific Research Publishing*, **9**, No. 3: 640 (2012).
23. V.R. Ryabov, *Steel Aluminizing* (Moskva: Metallurgiya: 1973), p. 240.
24. M. Brochu, J.G. Portillo, J. Milligan, and D.W. Heard, *The Open Surface Science Journal*, **3**: 105 (2011).
25. I.G. Brodova, I.G. Shirinkina, and Yu. P. Zaikov, *Physics of Metals and Metal Science*, **116**, No. 9: 928 (2015).
26. V.F. Danenko, L.M. Gurevich, and G.V. Ponkratova, *News of Volg GTU*. [*Problems of Material Science, Welding and Strength in Mechanical Engineering: Interuniversity. Collection of Scientific Articles*], **10**, No. 9 (136): 30 (2014).
27. V.I. Muraviev, P.V. Bakhmatov, N.G. Lonchakov, and S.Z. Chinilov, *Hardening Technologies and Coatings*, No. 11: 25 (2013).
28. M.A. Elizavetin, and E.A. Satel, *Technological Ways to Improve the Durability of Machines* (Moskva: Mashinostroenie: 1969), p. 400.
29. V.I. Kuzmin, A.A. Mikhal'chenko, and O.B. Kovalev, *Thermal Spray Technology*, **21**, No. 1: 159 (2012).
30. A.D. Pogrebnjak, V.I. Ivashchenko, P.L Skrynskyy, O.V. Bondar, P. Konarski, K. Zaleski, S. Jurga, and E. Coy, *Composites Part B-Engineering*, **142**: 85 (2018).
31. A.D. Pogrebnjak, A.A. Bagdasaryan, P. Horodek, V. Tarelnyk, V.V. Buranich, H. Amekura, N. Okubo, N. Ishikawa, and V.M. Beresnev, *Materials Letters*, **303**: 130548, (2021); https://doi.org/10.1016/j.matlet.2021.130548
32. G. Morand, P. Chevallier, L. Bonilla-Gameros, S. Turgeon, M. Cloutier, M. Da Silva Pires, A. Sarkissian, M. Tatoulian, L. Houssiau, and D. Mantovani, *Surface and Interface Analysis*, **53**, No. 7: 658 (2021); https://doi.org/10.1002/sia.6953
33. G. Maistro, S. Kante, L. Nyborg, and Y. Cao, *Surfaces and Interfaces*, **24**: 101093; https://doi.org/10.1016/j.surfin.2021.101093
34. V.G. Smelov, A.V. Sotov, and S.A. Kosirev, *ARPN Journal of Engineering and Applied Sciences*, **9**, No. 10: 1854 (2014).
35. B. Antoszewski, *IOP Conf. Ser.: Mater. Sci. Eng.*, **233** : 012036 (2017); https://doi.org/10.1088/1757-899X/233/1/012036
36. I. Pliszka and N. Radek, *Procedia Engineering*, **192**: 707 (2017); https://doi.org/10.1016/j.proeng.2017.06.122
37. B. Tarelnyk, O.P. Gaponova, Ye.V. Konoplyanchenko, N.S. Yevtushenko, and V.O. Herasymenko, *Metallofiz. Noveishie Tekhnol.*, **40**, No. 6: 795 (2018) (in Russian); https://doi.org/10.15407/mfint.40.06.0795
38. D.N. Korotaev, *Tekhnologicheskie Vozmozhnosti Formirovaniya Iznosostoikikh Nanostructur Ehlektroiskrovym Legirovaniem* [Technological Possibilities of Wear-Resistant Nanostructure Formation by Electric-Spark Alloying] (Omsk: SibADI: 2009) (in Russian).
39. A.D. Verkhoturov, *Formirovanie Poverkhnostnogo Sloya Metallov pri Ehlektroiskrovom Legirovanii* [Formation of the Metal Surface Layer by Electric-Spark Alloying] (Vladivostok: Dal'nauka: 1995) (in Russian).

40. V.B. Tarelnyk, O.P. Gaponova, V.B. Loboda, E.V. Konoplyanchenko, V.S. Martsinkovskii, Yu.I. Semirnenko, N.V. Tarelnyk, M.A. Mikulina, and B.A. Sarzhanov, *Surf. Engin. Appl. Electrochem*, **57**: 173 (2021); https://doi.org/10.3103/S1068375521020113
41. V.B. Tarelnyk, A.V. Paustovskii, and Y.G Tkachenko, *Electrode Materials for Composite and Multilayer Electrospark-Deposited Coatings from Ni–Cr and WC–Co Alloys and Metals. Powder Metall Met Ceram*, **55**: 585 (2017); https://doi.org/10.1007/s11106-017-9843-2
42. V. Martsynkovskyy, V. Tarelnyk, I. Konoplianchenko, O. Gaponova, and M. Dumanchuk, *Advances in Design, Simulation and Manufacturing II. DSMIE 2019. Lecture Notes in Mechanical Engineering* (Cham: Springer: 2020); https://doi.org/10.1007/978-3-030-22365-6_22
43. V.B. Tarel'nik, A.V. Paustovskii, Y.G. Tkachenko, V.S. Martsinkovskii, E.V. Konoplyanchenko, and B. Antoshevskii, *Surface Engineering and Applied Electrochemistry*, **53**, No. 3: 285 (2017); https://doi.org/10.3103/S1068375517030140
44. A.A. Ishchenko, *Technological Bases the Restoration of Industrial Equipment with Modern Polymeric Materials* (Mariupol: PSTU: 2007), p. 250.
45. V.S. Martsynkovskyi, *Sposib Obrobky Vkladyshiv Pidshypnykiv Kovzannia* [The Method of Processing the Liners of Sliding Bearings]: Patent 77906 UA. IPC, B23H1/00 (Bul. 1) (2007) (in Ukrainian).
46. V.S. Martsynkovskyi, V.B. Tarelnyk, O.H. Pavlov, and A.O. Ishchenko, *Sposib Vidnovlennia Znoshenykh Poverkhon Metalevykh Detalei (Varianty)* [The Method of Restoration of Worn Surfaces of Metal Parts (Variants)]: Patent 104664 UA. (Bul. 4) (2014) (in Ukrainian).
47. V.B. Tarel'nik, E.V. Konoplyanchenko, P.V. Kosenko, and V.S. Martsinkovskii, *Chemical and Petroleum Engineering*, **53**, Nos. 7–8: 540 (2017); https://doi.org/10.1007/s10556-017-0378-7
48. V. Dzyura, P. Maruschak, and O. Prentkovskis, *Algorithms*, **14**, No. 2: 46 (2021); https://doi.org/10.3390/a14020046
49. Yu.G. Schneider, *Precision Engineering*, **6**, No. 4: 219 (1984); https://doi.org/10.1016/0141-6359(84)90007-2
50. V. Martsinkovsky, V. Yurko, V. Tarelnik, and Yu. Filonenko, *Procedia Engineering*, **39**: 148 (2012); https://doi.org/10.1016/j.proeng.2012.07.019
51. V. Martsinkovsky, V. Yurko, V. Tarelnik, and Yu. Filonenko, *Procedia Engineering*, **39**: 157 (2012); https://doi.org/10.1016/j.proeng.2012.07.020
52. S.F. Vdovin, E.S. Makhnev, N.L. Mineeva, V.V. Tarasov, A.P. Andreev, *Elektron. Obrab. Mater.*, No. 6: 15 (1988) (in Russian).
53. S.M. Reshetnikov and S.F. Vdovin, *Elektronnaya Obrabotka Materialov*, **3**: 33 (1977).
54. A.V. Koval', *Surf. Engin. Appl. Electrochem.*, **58**: 176 (2022); https://doi.org/10.3103/S1068375522020041
55. S.A. Pyachin, A.A. Burkov, and V.S. Komarova, *Journal of Surface Investigation X-Ray Synchrotron and Neutron Studies*, **6**: 16 (2013).
56. V.B. Tarelnyk, V.S. Martsynkovskyi, O.P. Gaponova, Ye. Konoplianchenko, N.V. Tarelnyk, M.Yu. Dumanchuk, M.V. Honcharenko, B. Antoshevskyi, and Ch. Kundera, *Sposib Obrobky Poverkhon Stalevykh Detalei* [The Method of Processing the Surfaces of Steel Parts]: Patent 121346 UA. IPC B23H 1/06 (2006.01), B23H 9/00, C23C 12/02 (2006.01) (Bul. 9) (2020) (in Ukrainian).

57. O. Gaponova, Cz. Kundera, G. Kirik, V. Tarelnyk, V. Martsynkovskyy, Ie. Konoplianchenko, M. Dovzhyk, A. Belous, and O. Vasilenko, *Advances in Thin Films, Nanostructured Materials, and Coatings. Lecture Notes in Mechanical Engineering* (Singapore: Springer: 2019); https://doi.org/10.1007/978-981-13-6133-3_25
58. G.V. Kirik, O.P. Gaponova, V.B. Tarelnyk, O.M. Myslyvchenko, and B. Antoshevsky, *Powder Metallurgy and Metal Ceramics,* **56**, Nos. 11–12: 688 (2018); https://doi.org/10.1007/s11106-018-9944-6
59. V.B. Tarelnyk , O.P. Gaponova, and O.M. Myslyvchenko, *Metallofiz. Noveishie Tekhnol.*, **41**, No. 10: 1377 (2019); https://doi.org/10.15407/ mfint.41.10.1377
60. O.A. Bannykh, P.B. Budberg, and S.P. Alisova, *Diagrams of the State of Dual and Multicomponent Systems Based on Iron: Papers.* (Moskva: Metallurgy: 1986), p. 440 (in Russian).
61. Y.I. Mulyn and A.D. Verkhoturov, *Electrospark Alloying of Working Surfaces of Tools and Machine Parts with Electrode Materials Obtained from Mineral Raw Materials* (Vladivostok: Dal'nauka: 1999), p. 110 (in Russian).
62. D.V. Mironov, V.M. Mironov, V.F. Mazanko, D.S. Gertsriken, and P.V. Peretyatku, *Resource-Efficient Technologies*, **3**: 19 (2018); https://doi.org/10.18799/24056537/2018/3/199
63. V.F. Mazanko, D.S. Hertsryken, and V.M. Myronov, *International Conference 'Interaction of Radiation with Solids' (Sep. 23–25, 2015, Minsk)*, p. 240.
64. V.B. Tarelnik, B. Antoshevsky, and V.S. Martsinkovsky et al., *Cementation by Electroerosive Alloying* (Sumy: University Book: 2015), p. 233 (in Ukrainian).
65. V.S. Martsynkovskyi, V.B. Tarelnyk, and M.P. Bratushchak, *Sposib Tsementatsii Stalevykh Detalei Elektroeroziinym Leguvanniam* [Method for Carburizing of Steel Parts by Electroerosion Alloying], Patent 101715 UA. IPC 23N 9/00 (Bul., 8) (2013) (in Ukrainian).
66. A.N. Minkevich, *Chemical and Thermal Treatment of Metals and Alloys*, (Moskva: Mashinostroyenie: 1965), p. 493 (in Russian).
67. L.D. Plyatsuk, V.B. Tarelnyk, Cz. Kundera, O.V. Radionov, O.P. Gaponova. *Journal of Engineering Sciences*, **5**, No. 1: 16 (2018). https://doi.org/10.21272/jes.2018.5(1).c4
68. S.N. Khimukhin, *Structure and Properties of Metals and Alloys under Electrospark Action* (Khabarovsk: Pacific Publishing House. State University: 2015), p. 127 (in Russian).
69. N.B. Stavitskaya and B.I. Stavitsky, *Electronic Processing of Materials*, **1**:9 (1980).
70. L.S. Palatnik, *DAN USSR*, **89**: 455 (1953).
71. R. Johnson and G. Sheldon, *Journal of Vacuum Science& Technology A*, **4**, No. 6: 2740 (1986).
72. A.N. Ierusalimskaya, V.I. Samoilov, and P.I. Ulyakov, *Structural Changes in Substance under the Influence of Laser Pulses of Light*, **4**: 26 (1968).
73. V.B. Tarelnyk, E.V. Konoplyanchenko, O.P. Gaponova, and N.V. Tarelnik, *Ensuring the Protection of the Surfaces of End Pulse Seals of Turbomachines by Forming Wear-Resistant Nanostructures: Monograph* (Sumy: University Book: 2022), p. 252 (in Ukrainian).
74. B. Antoszewski, O.P. Gaponova, V.B. Tarelnyk, O.M. Myslyvchenko, P. Kurp, T. Zhylenko, and Ie. Konoplianchenko, *Materials*, **14**: 739 (2021); https://doi.org/10.3390/ma14040739

Received 26.01.2023;
in final version, 31.05.2023

В.Б. Тарельник[1], *О.П. Гапонова*[2], *Н.В. Тарельник*[1], *О.М. Мисливченко*[3]
[1] Сумський національний аграрний університет,
вул. Герасима Кондратьєва, 160, 40021 Суми, Україна
[2] Сумський державний університет,
вул. Римського-Корсакова, 2, 40007 Суми, Україна
[3] Інститут проблем матеріалознавства ім. І.М. Францевича НАН України,
вул. Омеляна Пріцака, 3, 03142 Київ, Україна

АЛІТУВАННЯ МЕТАЛЕВИХ ПОВЕРХОНЬ ЕЛЕКТРОІСКРОВИМ ЛЕҐУВАННЯМ

Проаналізовано вплив параметрів електроіскрового леґування алюмінійовим електродом на якість (шерсткість, мікроструктуру покриття, його суцільність, фазовий склад і мікротвердість) алітованого шару, оцінено вплив методів фінішного оброблення після алітування, вивчено жаротривкість одержаних покриттів. Металографічний аналіз показав, що покриття складаються з трьох ділянок: «білого» шару, дифузійної зони й основного металу. Зі збільшенням енергії розряду зростають такі параметри якости поверхневого шару як товщина, мікротвердість «білого» шару та перехідної зони, шерсткість. Суцільність «білого» шару за енергії розряду W_p = 0,52 Дж є низькою (50–60 %), з подальшим збільшенням енергії розряду зростає та за W_p = 6,8 Дж становить 100 %. Збільшення енергії розряду під час електроіскрового леґування (ЕІЛ) приводить до змін хемічного та фазового складів шару: за низьких енергій розряду формується шар, що складається переважно з α-Fe й оксидів Алюмінію. Зі збільшенням W_p шар складається з інтерметалідів заліза й алюмінію, а також вільного алюмінію, що підтверджується даними локального мікрорентґеноспектрального аналізу. Для практичного застосування можна рекомендувати процес алітування методом ЕІЛ з використанням режимів (енергія розряду в межах 4,6–6,8 Дж і продуктивність у 2,0–3,0 см^2/хв), які забезпечують формування «білого» шару завтовшки у 70–130 мкм, мікротвердістю у 5000–7500 МПа, шорсткістю (R_a) у 6–9 мкм і суцільністю у 95–100%. З метою збільшення товщини алітованого шару рекомендовано на крицеву поверхню попередньо наносити консистентну речовину, що містить алюмінійову пудру і, не чекаючи її висихання, проводити ЕІЛ алюмінійовим електродом. Тоді суцільність покриття складає 100%, товщина шару — до 200 мкм, мікротвердість — 4500 МПа. У роботі представлено результати дослідження параметрів якости багатокомпонентних алюмінійвмісних покриттів систем Al–S, Al–C–S, Al–C–B. Заміна алюмінійового електроду на графітовий призводить до пониження товщини та суцільности «білого» шару, відповідно, до 50 мкм і 30%. У свою чергу, мікротвердість на поверхні підвищується до 9000 МПа. Додавання до консистентної речовини 0,7 Бору приводить до збільшення товщини та суцільности «білого» шару, відповідно, до 60 мкм і 70%. Мікротвердість на поверхні збільшується до 12000 МПа. З метою пониження шерсткости поверхневого шару задля одержання суцільних покриттів рекомендується проводити ЕІЛ алюмінійовим електродом, але на менших режимах.

Ключові слова: електроіскрове леґування, покриття, алітування, мікротвердість, суцільність, шерсткість, структура, рентґеноструктурний аналіз, рентґеноспектральний аналіз.